Walter+Eliza Hall
Institute of Medical Research

Institute Research Publication Repository

This is author accepted version of :

Jeltsch KM, Hu D, Brenner S, Zoller J, Heinz GA, Nagel D, Vogel KU, Rehage N, Warth SC, Edelmann SL, Gloury R, Martin N, Lohs C, Lech M, Stehklein JE, Geerlof A, Kremmer E, Weber A, Anders HJ, Schmitz I, Schmidt-Supprian M, Fu M, Holtmann H, Krappmann D, Ruland J, Kallies A, Heikenwalder M, Heissmeye V. Cleavage of roquin and regnase-1 by the paracaspase MALT1 releases their cooperatively repressed targets to promote T17 differentiation. *Nature Immunology.* 2014 15(11):1079-108*,*

which has been published in final form at
doi:10.1038/ni.3008

The paracaspase Malt1 cleaves roquin and regnase-1 to release cooperative repression of mRNAs that promote T_H17 differentiation

Katharina M. Jeltsch[1,2]*, Desheng Hu[2]*, Sven Brenner[2,]*, Jessica Zöller[3], Gitta A. Heinz[2], Daniel Nagel[4], Katharina U. Vogel[2,5], Nina Rehage[1,2], Sebastian C. Warth[2], Stephanie L. Edelmann[1,2,], Renee Gloury[6], Nina Martin[2,7], Claudia Lohs[2], Lech Maciej[8], Jenny E. Stehklein[2], Arie Geerlof[9], Elisabeth Kremmer[2], Achim Weber[10], Hans-Joachim Anders[8], Ingo Schmitz[11,12], Marc Schmidt-Supprian[13], Mingui Fu[14], Helmut Holtmann[15], Daniel Krappmann[4], Jürgen Ruland[16], Axel Kallies[6], Mathias Heikenwalder[3] & Vigo Heissmeyer[1,2]

[1]Ludwig-Maximilians-Universität München, Institute for Immunology, Goethestr. 31, 80336 Munich, Germany

[2]Institute of Molecular Immunology, Research Unit Molecular Immune Regulation, Helmholtz Zentrum München, Marchioninistr. 25, 81377 Munich, Germany

[3]Institute for Virology, Technische Universität München/Helmholtz Zentrum München, Schneckenburgerstr. 8, 81675 Munich, Germany

[4]Institute of Toxicology and Pharmacology, Research Unit Cellular Signal Integration, Helmholtz Zentrum München, Ingolstädter Landstr. 1, 85764 Neuherberg, Germany

[5]present address: Laboratory of Lymphocyte Signalling and Development, Babraham Institute, Cambridge, CB22 3AT, UK

[6]The Walter and Eliza Hall Institute of Medical Research, 1G Royal Parade, Parkville Victoria, 3052 Australia

[7]present address: Johns Hopkins Bloomberg School of Public Health, Baltimore, MD 21205, USA

[8]Medizinische Klinik und Poliklinik IV, Ludwig-Maximilians-Universität München, Ziemssenstr. 1, 80336 München, Germany

[9]Institute of Structural Biology, Helmholtz Zentrum München, Ingolstädter Landstr. 1, 85764 Neuherberg, Germany

[10]Institute for Surgical Pathology, University Hospital, Schmelzbergstr. 12, 8091 Zürich, Switzerland

[11]Helmholtz Centre for Infection Research, Inhoffenstr. 7, 38124 Braunschweig, Germany

[12]Institute for Molecular and Clinical Immunology, Otto-von-Guericke-Universität Magdeburg, Leipziger Strasse 44, 39120 Magdeburg, Germany

[13]Max Planck Institute of Biochemistry, Am Klopferspitz 18, 82152 Martinsried, Germany

[14]Department of Basic Medical Science, School of Medicine, University of Missouri-Kansas City, 2411 Holmes Street, Kansas City, MO 64108, USA

[15]Institute of Biochemistry, Hannover Medical School, Carl-Neuberg Str.1, 30623 Hannover, Germany

[16]Institut für Klinische Chemie und Pathobiochemie, Klinikum rechts der Isar, Technische Universität München, Ismanninger Str. 22, 81675 Munich, Germany

*equally contributing authors

contact information: Institute for Immunology, Ludwig-Maximilians-Universität München, Goethestr. 31, 80336 Munich, Germany, Phone: +49 89 2180 75629, Fax: +49 89 2180 75629, vigo.heissmeyer@med.uni-muenchen.de

Abstract

Humoral autoimmunity paralleled by the accumulation of T_{FH} cells has been linked to mutation in the RNA-binding protein roquin-1. Here, we show that absence of roquin proteins in T cells caused pathology and accumulation of T_H17 cells in the lung. Roquin inhibited T_H17 differentiation and cooperated with the endoribonuclease regnase-1 in the repression of target mRNAs that encode the T_H17-promoting factors *Il6*, *Icos, cRel, Irf4*, *Nfkbid* and *Nfkbiz*. The cooperation required RNA-binding by roquin and the nuclease activity of regnase-1. Upon antigen recognition by the T cell receptor (TCR) roquin and regnase-1 proteins were cleaved by the paracaspase Malt1. The system worked as a 'rheostat' by translating TCR signal strength via graded inactivation of post-transcriptional repressors and differential derepression of targets into enhanced T_H17 differentiation.

Introduction

Gene regulation on the post-transcriptional level exerts essential control over immune responses. This becomes evident from mice with mutations in the gene *Rc3h1* encoding roquin-1 or in the gene *Zc3h12a* encoding regnase-1 (also called Mcpip1). These mice develop severe autoimmune or auto-inflammatory diseases[1, 2, 3, 4]. Post-transcriptional regulation can switch immune responses by changing the efficiency of translation or stability of mRNA for selected genes. Prominent examples include ligands or receptors in the signaling pathways of cytokines, chemokines as well as costimulation[5]. Roquin-1 and roquin-2 are RNA-binding proteins that recognize *Icos*, *Ox40* and *Tnf* mRNAs and decrease their half-life[6, 7, 8, 9]. Regnase-1 negatively regulates expression of *Il6*, *Il12b*, *Il2*, *Icos*, *Ox40*, *Ctla4* and *cRel* as well as its own mRNA *Zc3h12a*[1, 10, 11]. Regnase-1 is an endonuclease that cleaves target mRNAs or the terminal loop of pre-miRNAs *in vitro*[1, 12]. The regnase-1-mediated repression was mapped to regions in the 3' UTRs of *Il6*, *cRel* and *Zc3h12a* mRNAs that have the potential to form stem-loop structures[1, 10, 11]. However, a specific consensus sequence or structure for regnase-1-recognized *cis*-elements has not been defined. A search for factors that regulate the half-life of *Tnf* mRNA recently identified the binding of roquin-1 and its paralog roquin-2 to a constitutive decay element (CDE) in the *Tnf* 3' UTR[7]. A consensus stem-loop structure in the CDE was bound through the amino-terminal ROQ domain of roquin-1[7, 13, 14] and the recognition of this *cis*-element was shown to be required and sufficient to induce roquin-mediated mRNA decay[7]. Whether the activity of roquin is constitutive or can be regulated remained elusive. In contrast, regnase-1 is known to be regulated on several levels. In T cells, the protein is cleaved by the Malt1 paracaspase after T cell and costimulatory receptor stimulation[11]. Malt1 is part of the Carma1/Bcl10/Malt1 (CBM) complex and has scaffold function as well as protease activity[15, 16]. While the intact

CBM complex is required for canonical NF-κB signaling induced by the antigen receptor[17], the catalytic activity cleaves targets such as Bcl10, A20, Cyld and RelB and may thereby modulate canonical and alternative NF-κB[15, 16, 18, 19] as well as JNK signaling[20]. Interestingly, the presence of Malt1 in dendritic and $CD4^+$ T cells appears critical for T_H17 differentiation and Malt1-deficient mice are resistant to experimentally-induced autoimmune encephalomyelitis (EAE)[21, 22, 23]. Consistent with an importance of the enzymatic activity of Malt1, the pharmacologic inhibition of the paracaspase was recently shown to attenuate the development of EAE[24].

Regnase-1-deficient mice show severe anemia, postnatal death, accumulation of effector T cells, increased immunoglobulin levels, production of autoantibodies and severe systemic inflammation[1]. Initially, these phenotypes were related to impaired control of innate immune responses via deregulation of regnase-1 targets IL-6 and IL-12p40[1]. However, recent work has shown that combined deficiencies of *Zc3h12a* and *IL6* or *Zc3h12a* and *IL12p40* did not rescue the phenotype[11]. Instead, T cell-intrinsic functions of regnase-1 were required to prevent autoimmune and auto-inflammatory phenotypes[11]. Interestingly, a number of phenotypes and functions, most prominently (i) the activation of T and B lymphocytes, (ii) the derepression of Icos and Ox40 levels, (iii) the development of autoantibodies, (iv) the postnatal lethality and (v) the disrupted splenic microarchitecture resemble phenotypes of mouse models with roquin mutations[1, 2, 3, 8, 11, 25]. Despite such overlap a connection between these pathways has not been established so far. Here, we demonstrate the convergence of roquin- and regnase-1-mediated post-transcriptional gene regulation in the control of T_H17 differentiation.

Results

Lung pathology in mice that lack roquin proteins in T cells

We have recently uncovered functional redundancy of roquin paralogs. This became evident in mice with T cell-specific combined ablation of *Rc3h1* and *Rc3h2* genes encoding roquin-1 and roquin-2 proteins, respectively[8]. Analyzing these *Rc3h1-2$^{fl/fl}$; Cd4-cre* mice between 7 and 30 weeks of age revealed prominent lung pathology. We found a progressive reduction of the alveolar space concomitant with inflammation (**Fig. 1a–b, Supplementary Fig. 1a**). In the lungs of *Rc3h1-2$^{fl/fl}$; Cd4-cre* mice we determined infiltrations of CD45$^+$ hematopoietic cells (**Supplementary Fig. 1b**) and increased numbers of CD3$^+$ T cells (**Fig. 1b–c, Supplementary Fig. 1a,c**). Moreover, MHCII$^+$ antigen presenting cells were overrepresented (**Fig. 1b–c, Supplementary Fig. 1a,d**). Staining with Ki67-specific antibodies revealed increased proliferation of cells in the lungs of *Rc3h1-2$^{fl/fl}$; Cd4-cre* mice (**Fig. 1b–c, Supplementary Fig. 1a,e**). The pathology of the lung in *Rc3h1-2$^{fl/fl}$; Cd4-cre* mice also showed increased numbers of mucin-producing goblet cells (**Fig. 1d–e**), presumably in response to the progressive airway insult. In addition, we detected a thickening of the artery walls (**Fig. 1f**) and the deposition of collagen (**data no shown**). Consistent with the observed pathology in older *Rc3h1-2$^{fl/fl}$; Cd4-cre* mice we observed reduced viability with an average survival of 130 days (**Supplementary Fig. 1f**).

Roquin-deficiency does not induce autoantibodies against lung antigens

Analyzing humoral autoimmunity in *Rc3h1-2$^{fl/fl}$; Cd4-cre* mice, we did not detect autoantibodies against lung antigens (**Fig. 1g**). Despite accumulation of T_{FH} cells[8], the majority of sera from *Rc3h1-2$^{fl/fl}$; Cd4-cre* mice lacked IgG-reactivity in immunoblots with tissue proteins from immunodeficient mice. In contrast many different reactivities were detected in sera from *sanroque* mice that express the point-mutated (M199R) form of roquin-1 or in sera from *MRL$^{lpr/lpr}$* mice that overexpress Fas ligand and also develop lupus-like autoimmune disease[3, 26] (**Fig.**

1g). Different from *MRL*$^{lpr/lpr}$ and *sanroque* mice, *Rc3h1-2*$^{fl/fl}$*; Cd4-cre* mice also did not exhibit anti-nuclear antibodies[8], anti-DNA antibodies and rheumatoid factor (**Supplementary Fig. 1g-h**). Interestingly, the sera of several *Rc3h1-2*$^{fl/fl}$*; Cd4-cre* mice displayed strong reactivity against pancreatic antigens, proving that they have the potential to develop autoantibodies (**Fig. 1h**). The apparent lack of humoral reactivity against typical autoantigens may be explained by the perturbed splenic microarchitecture that is observed in *Rc3h1-2*$^{fl/fl}$*; Cd4-cre* mice[8]. Nevertheless, the lung pathology in *Rc3h1-2*$^{fl/fl}$*; Cd4-cre* mice points at an important function of roquin in T cells that is different from T_{FH}-mediated B cell help.

Control of T_H17 differentiation by roquin proteins

Investigating cytokine levels we found strongly increased concentrations of IL-17 and IL-6 in the sera of *Rc3h1-2*$^{fl/fl}$*; Cd4-cre* mice (**Fig. 2a–b**), while TNF and IL-10 levels were moderately increased (**Fig. 2c–d**). Interestingly, IFN-γ, which is known to be elevated in the sera of *sanroque* mice[27], was not increased in *Rc3h1-2*$^{fl/fl}$*; Cd4-cre* mice (**Fig. 2e**). In line with our ELISA data, *ex vivo* stimulation revealed a much higher frequency of IL-17-producing $CD4^+$ T cells isolated from lymph node and especially from the lung of *Rc3h1-2*$^{fl/fl}$*; Cd4-cre* compared to wild-type mice (**Fig. 2f**). $CD4^+$ T cells from the lung of *Rc3h1-2*$^{fl/fl}$*; Cd4-cre* mice did not show increased production of the T_H2 cytokine IL-4 (**Supplementary Fig. 2a**). The predominant IL-17 production by $CD4^+$ T cells from the lung of *Rc3h1-2*$^{fl/fl}$*; Cd4-cre* mice correlated with an increased frequency of cells expressing the RORγt transcription factor (**Supplementary Fig. 2b**), and most of the IL-17-producing cells also expressed the chemokine receptor CCR6 (**Supplementary Fig. 2c**). The increase of T_H17 cells in the lung of *Rc3h1-2*$^{fl/fl}$*; Cd4-cre* mice was paralleled by an increased frequency and number of neutrophils (Gr-1^+ F4/80^-) (**Fig. 2g** and **data not shown**). In agreement with our *in vivo* results, $CD4^+$ T cells lacking both roquin proteins showed a

pronounced bias toward T_H17 differentiation (**Fig. 2h**). When naive $CD4^+$ T cells were cultured under T_H17 conditions, restimulations induced twice as many IL-17 producers in cells from *Rc3h1-2$^{fl/fl}$; Cd4-cre* compared to wild-type mice (**Fig. 2h**). Consistently, the reciprocal differentiation program into $Foxp3^+$ Treg cells was moderately impaired (**Fig. 2i**). Naive $CD4^+$ T cells from *Rc3h1-2$^{fl/fl}$; Cd4-cre* mice stimulated either under T_H1 or T_H0 conditions showed a trend toward enhanced T_H1 differentiation as measured by the frequency of IFN-γ-producing cells, and less IL-4-producing cells were determined in restimulated T_H2 cultures (**Fig. 2j**,**k**). Given the prominent involvement of T_H17 cells in psoriasis, colitis and arthritis we also analyzed histology sections of skin, intestine and joints of *Rc3h1-2$^{fl/fl}$; Cd4-cre* and wild-type mice (**Supplementary Fig. 2d-i**). We did not find significant abnormalities in the skin (**Supplementary Fig. 2d-e**) or small and large intestine (**Supplementary Fig. 2f-g and data not shown**). In addition, the morphology of the joints was normal and showed no signs of arthritis (**Supplementary Fig. 2h**). However, flow cytometric analyses of $CD4^+$ T cells from the small and large intestine of *Rc3h1-2$^{fl/fl}$; Cd4-cre* mice showed an enhanced frequency of IL-17^+ single and IL-17^+/IFN-γ^+ double producing $CD4^+$ T cells compared to wild-type counterparts (**Supplementary Fig. 2i**). Furthermore, pronounced infiltration of $CD3^+$ and $CD45^+$ cells was present in the stomach, which correlated with a strong nuclear p-STAT3 signal that was predominantly observed in epithelial cells (**Fig. 2l-m**). These data uncover a previously unrecognized cell-intrinsic role of roquin proteins in the control of T_H17 differentiation, accumulation of T_H17 cells in the lung and gut as well as in the development of lung inflammation and gastritis.

Regulation of roquin proteins by Malt1 cleavage

Having shown that roquin-1 and -2 control T cell differentiation, we asked whether their protein levels are regulated. T cell stimulation caused the disappearance of full-

length roquin-1 and -2 proteins (**Fig. 3**). Specifically, as early as 30 min after stimulation of wild-type $CD4^+$ T cells with PMA/ionomycin the amounts of roquin-1 and roquin-2 full-length proteins were reduced and almost no full-length roquin-1 and roquin-2 proteins were detected in cell extracts after 60 min of treatment (**Fig. 3a**). In these immunoblots with a monoclonal antibody that equally recognizes both roquin paralogs[8] we also detected several faster migrating bands of approximately 50-60 kDa. These bands were only weakly recognized in extracts of unstimulated cells, but increased in intensity between 10-30 min and remained constant between 30-180 min of stimulation (**Fig. 3a**). In $CD4^+$ T cells from individual roquin-1 and -2 knockouts, the full-length protein similarly disappeared upon stimulation and one faster migrating band of roquin-1 or roquin-2 appeared (**Fig. 3b**). Similarly, extracts of naive human $CD4^+$ T cells showed full-length ROQUIN proteins only in unstimulated cells and an appearance of truncated versions upon PMA/ionomycin-stimulation (**Fig. 3c**). We determined that stimulation of cells with PMA alone was sufficient to induce the observed changes (**Fig. 3d**). The pharmacologic agents PMA and ionomycin mimic very strong TCR activation and costimulation. Consistent with this notion, combined anti-CD3/anti-CD28 stimulation also induced the faster migrating roquin bands (**Fig. 3e**), while stimulation with anti-CD28 or anti-CD3 alone was less effective (**Fig. 3e**). Furthermore, stimulation of SMARTA TCR-transgenic $CD4^+$ T cells with antigen-presenting cells and cognate antigen induced faster migrating roquin bands by 8h or 16h of stimulation (**Fig. 3f**). During these long-term stimulations with potentially weaker TCR agonists we observed the reappearance of the full-length band at later times consistent with protein re-synthesis and incomplete proteolysis. We tested degradation of roquin proteins by the proteasome or cleavage by caspases (**Fig. 4a**). PMA/ionomycin-induced roquin cleavage was partially or completely inhibited by preincubation of cells with inhibitors for the Malt1 paracaspase, including a peptide inhibitor (z-VRPR-fmk) as well as Mepazine and Thioridazine, two recently described pharmacologic inhibitors for this paracaspase[28]

(**Fig. 4a**). In contrast, the proteasome inhibitor (MG132) and an inhibitor of effector caspases (Ac-DEVD-CHO) had no effect. Consistent with a critical role for Malt1 in roquin cleavage also Malt1-deficient T cells did neither show decreased amounts of the full-length nor roquin cleavage products upon PMA/ionomycin stimulation (**Fig. 4b**). Since Malt1 is an arginine-specific protease, we tested candidate arginine residues in roquin-1. We retrovirally overexpressed human MALT1 in *Malt1*$^{-/-}$ MEF cells together with roquin-1 wild-type or roquin-1^{R510G} mutant proteins. MALT1 overexpression is able to activate the paracaspase activity presumably by favoring the formation of dimers[29]. Expression of Roquin-1^{WT} protein showed two truncated fragments (**Fig. 4c**, left panel). The faster migrating band was eliminated by expression of a roquin-1^{R510G} protein that instead enhanced the slower migrating cleavage product (**Fig. 4c**, left panel). Consistently, expression of a roquin-1$^{1-510}$ fragment showed one band that co-migrated with the faster migrating product (**Fig. 4c**, left panel). These findings proved that Malt1 cleaves roquin-1 preferentially after arginine 510. The alternative cleavage site was eliminated by mutation of arginine 579, while mutation of arginine 560 or arginine 488 had no effect (**Fig. 4c**). The cleavage bands that comigrated with roquin-1$^{1-510}$ and roquin-1$^{1-579}$ did not appear when a mutant with combined amino acid exchanges, roquin-1$^{R510G/R579G}$, was expressed (**Fig. 4d**, right panel). They were also not produced when the catalytically inactive MALT1 protein (PM) was used for reconstitution of *Malt1*$^{-/-}$ MEF cells (**Fig. 4d**, right panel). We then confirmed direct cleavage of roquin-1 through the Malt1 paracaspase by incubating a catalytically active GST-MALT1 fusion protein with the recombinant full-length roquin-1 protein. Immunoblots showed that the *in vitro* cleavage reaction decreased the levels of full-length protein and led to the appearance of a main cleavage fragment of approximately 55 kDa that comigrated with roquin-1$^{1-510}$ expressed in 293T cells (**Fig. 4e**). The enzymatic cleavage was specific, since it was blocked by the specific peptide inhibitor z-VRPR-fmk (**Fig. 4e**).

We then reconstituted roquin-1 expression in naive roquin-1 and roquin-2 double-deficient CD4$^+$ T cells. To this end we isolated cells from *Rc3h1-2$^{fl/fl}$; CAG-CAR$^{stop\text{-}fl}$; Cd4-cre* mice that are susceptible to adenoviral gene transfer due to transgenic coxsackie adenovirus receptor (CAR) expression[8]. Comparing cells with equal GFP expression (**Supplementary Fig. 3a**) we found that ectopic expression of the roquin-1$^{R510G/R579G}$ mutant was more effective in downregulating expression of Icos, a known target of roquin in CD4$^+$ T cells, than roquin-1^{WT} (**Fig. 4f**). Expression of the cleavage product (roquin-1$^{1\text{-}510}$) did not affect Icos expression (**Fig. 4f**), confirming our previous observation that carboxy-terminal sequences are required for post-transcriptional repression[6, 8]. Immunoblots with antibodies against a carboxy-terminal epitope of roquin-1 detected an endogenous carboxy-terminal cleavage product induced by T cell stimulation with PMA/ionomycin (**Supplementary Fig. 4b**). These data are consistent with a preferential cleavage of roquin-1 by Malt1 at the LIPR^{510}GTD site and an alternative cleavage at MVPR^{579}GSQ. While both roquin-1 sites are conserved in mouse and human, only the first cleavage site of roquin-1 is present in mouse roquin-2 (LIPR^{509}GTD) and conserved in its human ortholog (LISR^{509}TDS) (**Fig. 4g**). All ROQUIN cleavage sites showed extensive homology to target sites in regnase-1 and RelB proteins and lesser homology to A20, BCL-10, NIK and CYLD (**Fig. 4g**). To test whether the absence of roquin proteins changed the cleavage of other Malt1 targets we acutely deleted *Rc3h1* and *Rc3h2* genes in T_H17 cells (**Fig. 4h**). Transduction with cre recombinase-encoding retroviruses strongly reduced roquin protein levels in CD4$^+$ T cells from *Rc3h1-2$^{fl/fl}$* mice. This acute deletion of *Rc3h1-2* genes did not prevent cleavage of Cyld or regnase-1 upon PMA/ionomycin stimulation (**Fig. 4h**). Surprisingly, the regnase-1 protein exhibited strong upregulation in cells with acute deletion of *Rc3h1-2* genes suggesting that regnase-1, which is known to regulate expression of its own *Zc3h12a* mRNA, is also under the control of roquin proteins.

Roquin and regnase-1 cooperate in post-transcriptional gene regulation

The extensive overlap between roquin and regnase-1 functions prompted us to ask whether regnase-1 and roquin-1 regulate the same set of target mRNAs. In fact, for the known targets of regnase-1 *Il6*, *Zc3h12a*, *cRel* and *Ctla4*[11], we determined negative regulation also by roquin (**Fig. 4h**, **5a-d**). Importantly, reconstitution of MEF cells deficient for roquin- and regnase-1, respectively, with doxycyclin-inducible forms of these genes (**Supplementary Fig. 4a–b**) repressed the IL-17 and TNF-induced IL-6 production (**Fig. 5a**). Acute deletion of roquin-encoding genes by retroviral cre recombinase transduction of $CD4^+$ T cells from *Rc3h1-2*$^{fl/fl}$ mice not only effectively induced Irf4 protein levels[8], but also increased c-Rel protein expression compared to wild-type cells (**Fig. 5b**). Besides elevated surface expression of Icos and Ox40 we also found increased intracellular Ctla-4 protein after culturing naive $CD4^+$ T cells from *Rc3h1-2*$^{fl/fl}$*; Cd4-cre* mice under T_H17 conditions (**Fig. 5c**). We then demonstrated that regnase-1 also regulated the predicted roquin mRNA target *Nfkbid* (encoding IκBNS) that contains two CDE sequences in its 3' UTR[7] (**Fig. 5d**). Analyzing IκBNS expression in MEF cells revealed strongly enhanced protein expression not only in roquin- but also in regnase-1-deficient cells, while wild-type counterparts exhibited very low protein amounts (**Fig. 5d**). We then experimentally established *cRel*, *Ctla4, Il6* and *Irf4* mRNAs as new post-transcriptional targets of roquin-1 (**Fig. 5e**) and demonstrated Irf4 as a new target for regnase-1 (**Fig. 5f**). We used MEF cells that were either deficient for roquin (**Fig. 5e**) or regnase-1 (**Fig. 5f**) but can be reconstituted with doxycyclin-inducible roquin-1 or regnase-1, respectively (**Supplementary Fig. 4a-c**). Before induction, these cells were infected with retroviruses containing an *ICOS* reporter gene that was either expressed without (CDS) or with different 3' UTRs of selected target genes. Inducing roquin-1 (**Fig. 5e**, red histogram) or regnase-1 (**Fig. 5f**, blue histogram) did not change the ICOS surface expression generated from constructs without 3' UTR (**Fig. 5e–f,** *CDS*). In

contrast, ICOS expression was substantially decreased by roquin-1 or regnase-1 induction when the *ICOS* reporter gene was fused to its own 3' UTR (**Fig. 5e–f**). Similar post-transcriptional repression by roquin-1 and regnase-1 was observed for the 3' UTRs of *Ctla4* and *cRel,* while the 3' UTRs of *Il6* and *Irf4* were moderately inhibited (**Fig. 5e–f**). Since the ICOS reporter fused to the 3' UTRs of *Nfkbiz* and *Nfkbid* were already fully repressed in wild-type cells, we tested the effect of roquin depletion ([13] and **Supplementary Fig. 5d-e**). Both reporters were derepressed in a MEF cell line upon tamoxifen-induced activation of a Cre-ERT2 fusion protein that deleted the roquin-1- and roquin-2-encoding alleles (**Fig. 5g**). This derepression was much stronger than for the 3' UTRs of ICOS and *Irf4* (**Fig. 5g**). Together, these gain- or loss-of-function experiments uncover differential regulation of 3' UTRs of target mRNAs that are shared by roquin and regnase-1.

We showed functional cooperation of roquin-1 and regnase-1 in the regulation of target mRNAs by coexpressing the *ICOS* reporter in the context of its own 3' UTR with individual or both effectors. We used a wild-type MEF cell clone that, besides stably expressing ICOS, also expressed doxycyclin-inducible roquin-1-P2A-mcherry. After retroviral superinfection of these cells with regnase-1-IRES-Thy1.1, the cells were left untreated or were induced to express roquin-1. ICOS levels were similarly downregulated by individual expression of regnase-1 or roquin-1. However, the downregulation was more pronounced in cells that co-expressed regnase-1 and roquin-1 (Thy1.1^{+}; mcherry^{+}) (**Fig. 6a**). These findings indicated additive or potentially cooperative effects of both regulators in the repression of ICOS (**Fig. 6a**). We then demonstrated interdependence of roquin and regnase-1 in post-transcriptional regulation (**Fig. 6b**). In these experiments we first transduced roquin- (**Fig. 6b**, upper panel) or regnase-1-deficient MEF cells (**Fig. 6b**, lower panel) with a vector encoding the *ICOS* reporter gene fused to the most 3' 260 nts region from the *Tnf* 3' UTR[13]. We then transduced the cells with a roquin-1-IRES-Thy1.1 (**Fig. 6b**, left panel, red

histograms) or with a regnase-1-IRES-Thy1.1 retrovirus (**Fig. 6b**, right panel, blue histograms). Importantly, the reconstitution of roquin-deficient or of regnase-1-deficient cells was equally able to downregulate reporter expression (**Fig. 6b**, upper left and lower right panels). In contrast, the overexpression of roquin-1 in regnase-1-deficient cells and the overexpression of regnase-1 in roquin-deficient cells had no or only little effect on the expression of the reporter (**Fig. 6b**, upper right and lower left panels). To define the requirements in regnase-1 for cooperation with roquin we introduced point mutations in regnase-1 that have been shown to interfere with its nuclease function (D225A D226A), its deubiquitinase function (C157A) or with both (D141N) (**Supplementary Fig. 4f** and [1, 30]). All mutant and wild-type regnase-1 proteins depended on the presence of roquin (**Fig. 6c**, upper panel). Reconstituting regnase-1-deficient cells with wild-type or mutant forms of regnase-1 revealed a requirement for the nuclease but not for the deubiquitinase activity (**Fig. 6c**, lower panel). Analyzing downregulation of the CDE-controlled ICOS reporter by wild-type and mutant forms of roquin-1 (**Supplementary Fig. 4g** and [13]), we found again no regulation in regnase-1-deficient cells (**Fig. 6d**, lower panel). As expected expression of wild-type roquin-1 in roquin-deficient cells, inhibited the reporter. In contrast, mutations that partially (K239A R260A) or more completely (K220A K239A R260A) interfered with roquin-1 binding to CDE structures diminished reporter repression. We then fused a region that contained the ROQ domain of roquin-1 to the full-length regnase-1 open reading frame (**Fig. 6e and Supplementary Fig. 4h**). This fusion protein was not only as active as wild-type regnase-1 in regnase-1-deficient cells (**Fig. 6f**, lower panel), it also became cooperation-independent and downregulated the reporter in roquin-deficient cells (**Fig. 6f**, upper panel). Together, these findings show that the cooperation is defined through functional interaction of the RNA-binding and nuclease activities of roquin-1 and regnase-1, respectively.

Expression levels of IκBNS and IκBζ control T_H17 differentiation

We then tested the importance of roquin and regnase-1 gene regulation in T_H17 differentiation. First, we showed that reducing the cellular amounts of regnase-1 strongly promoted T_H17 differentiation (**Fig. 7a**). Infecting naive TCR-transgenic $CD4^+$ T cells with adenoviruses that encode *Zc3h12a*-specific shRNAs and coexpress GFP, we found an efficient reduction of regnase-1 protein and increased protein expression of the regnase-1 target IκBζ in purified GFP^{hi} cells (**Supplementary Fig. 5a-b**). To test the impact of IκBζ or IκBNS regulation by roquin and regnase-1 proteins on T_H17 differentiation we decreased the cellular levels of both proteins by two different shRNAs (**Supplementary Fig. 5c-d**). Similar to IκBζ, which was shown previously to be required for IL-17 production[31], knockdown of IκBNS markedly decreased IL-17 production, uncovering a previously unrecognized T_H17-promoting effect of IκBNS (**Fig. 7a)**. The effect was specific, because we did not find regulation of IFN-γ-producing cells under T_H1 conditions (**Fig. 7b**). Consistent with these results, when we expressed *Nfkbiz*- or *Nfkbid*-specific shRNAs in roquin-1 and roquin-2-deficient $CD4^+$ T cells their increased T_H17 differentiation was partially normalized (**Fig. 7c–d**). These finding showed that the increased differentiation observed in roquin-deficient T cells was, at least in part, mediated through the upregulation of IκBζ and IκBNS. A similar knockdown of regnase-1 in roquin-deficient T cells still increased IL-17-producing cells (**Fig. 7e),** indicating that roquin and regnase-1 not only have redundant functions. Reconstitution of roquin-deficient T cells with roquin-1-expressing adenoviruses normalized increased differentiation (**Fig. 7f**). Importantly, the Malt1-insensitive mutant of roquin-1 (roquin-$1^{R510G/R579G}$) showed enhanced activity to reduce the frequency of IL-17-producing cells, while expression of the Malt1-induced cleavage product (roquin-1^{1-510}) showed no effect (**Fig. 7f**).

We then established that the targets IκBζ, IκBNS and Irf4 are placed under critical post-transcriptional regulation in T cells downstream of Malt1 (**Fig. 8a–b**).

Stimulations of wild-type $CD4^+$ T cells with PMA and ionomycin induced strong expression of IκBζ between 30-120 min and continuously increasing expression of IκBNS and Irf4 between 60 and 180 min. This upregulation of roquin and regnase-1 targets closely followed the cleavage of roquin and regnase-1 proteins, which was complete after 30 min (**Fig. 8a**). In fact, pretreatment of cells with the Malt-1 paracaspase inhibitor Mepazine not only inhibited roquin and regnase-1 cleavage, but also prevented the induction of IκBζ, IκBNS and Irf4 after 60 min of stimulation (**Fig. 8b**).

We then linked TCR signal strength to the cleavage of post-transcriptional regulators, target derepression and differentiation decisions (**Fig. 8c-h**). Stimulating OTII TCR-transgenic T cells with increasing amounts of cognate $OVA_{323-339}$ peptide led to the accumulation of roquin cleavage fragments and an induction of Irf4 (**Fig. 8c**). In contrast stimulation with mutant $OVA_{323-339}$ peptides that show decreased affinity (R9, low and F9, very low) for the OTII transgenic TCR[32] revealed reduced or even absent cleavage of roquin (**Fig. 8d**). Single cell analyses of Irf4 in activated T cells ($CD4^+CD69^+$) confirmed a graded Irf4 expression that positively correlated with TCR avidity (**Fig. 8e**) and TCR affinity (**Fig. 8f**). Importantly we found increased frequencies of IL-17-producing cells when OTII cells were stimulated with increasing concentrations of wild-type peptide (**Fig. 8g**), while stimulation with the mutant peptide (R9) yielded in much lower frequencies of IL-17 producing cells (**Fig. 8h**). Thus roquin cleavage and T_H17 differentiation were positively correlated with TCR signal strength. Together these data support a model in which TCR signal strength is translated into a graded activity of Malt1, graded proteolytic inactivation of roquin and regnase-1 and differential derepression of their post-transcriptional targets that promote T_H17 differentiation.

Discussion

We have identified the cooperation of roquin and regnase-1 in post-transcriptional gene regulation by demonstrating co-regulation of 3' UTRs of overlapping target mRNAs. Our results indicate that regnase-1 contributes through its nuclease activity while the RNA-binding activity of roquin was required and sufficient for cooperative target repression. Cleavage by the paracaspase Malt1 has been shown to inactivate regnase-1[11]. Our results show that it also cleaves and inactivates roquin-1 and -2 proteins and releases target mRNAs of roquin and regnase-1 from repression. We cannot exclude a potential dominant negative function of the amino-terminal cleavage product of roquin-1, however, ectopic expression was unable to regulate Icos levels or T_H17 differentiation[6, 8].

The combined T cell-specific loss of roquin-1 and roquin-2 resulted in inflammation and lung pathology and an overexpression of T helper cell cytokines, in particular IL-17. This was reminiscent of ectopic expression of a hyperactive Stat3 protein in peripheral T cells, which similarly induced the accumulation of T_H17 cells in the lung and was associated with the attraction of neutrophils[33]. The changes in the lung in both mouse models included the thickening of the airway epithelium and increased mucus production and were associated with decreased viability[33]. Naive $CD4^+$ T cells from both models revealed enhanced T_H17 differentiation and IL-17 levels were elevated in the sera[33]. The importance of IL-17 for the pathology and viability was demonstrated by injection of IL-17–neutralizing antibodies into mice expressing hyperactive Stat3 in T cells[33]. One explanation for the selective pathology in the lung is that air-borne antigens may enable effective priming and differentiation of T_H17 cells. This is consistent with the observation that the hyperactive Stat3 molecules still depend on the initial T cell activation before being locked into the hyperactive state that drives differentiation. We have also observed a gastritis phenotype in mice that lack roquin in T cells. Although this phenotype could again relate to special conditions for priming and differentiation of T cells in this barrier organ, stomach

antigens could also be targets of autoantibodies as it has recently been reported for the gastritis phenotype that develops in regnase-1–deficient mice[4].

The selective differentiation toward T_{FH}, T_H1 and T_H17 upon roquin loss-of-function may be due to shared requirements for TCR signaling strength. We show that post-transcriptional regulation by roquin and regnase-1 converges on the regulation of target mRNAs that promote T_H17 differentiation, many of which also affect T_H1 and T_{FH} decisions. Most upstream is the repression of mRNAs encoding cytokines including TNF and IL-6. Loss of roquin thereby leads to overproduction of IL-6 that will drive T_H17 differentiation and impair induction of Treg cells[34]. Increased TNF and IL-17 levels induce further IL-6 production in epithelial cells and fibroblasts. A second layer of targets represents inducible costimulators ICOS, Ox40 and CTLA-4, among which ICOS has also been shown to be important for T_H17 cell expansion[35]. We have also identified post-transcriptional regulation by roquin and regnase-1 of the transcription factors Irf4 and c-Rel as well as of the transcription modulators IκBNS and IκBζ. IκBζ expression was required and overexpression was sufficient to promote T_H17 differentiation, and IκBζ cooperated with RORα and RORγt to enhance IL-17 expression[31]. Our knockdown results indicated that IκBNS was similarly important for T_H17 differentiation as IκBζ. IκBNS has not been involved in T_H17 function so far, but was shown to cooperate with the transcription factor c-Rel in the development of $Foxp3^-$ Treg precursors in the thymus[36]. c-Rel itself is critical for the differentiation of T_H17 cells and c-Rel-deficient mice are resistant to EAE[37, 38, 39]. Finally, the transcription factor Irf4 is required for T_H17 differentiation[47]. We have established that Malt1-mediated cleavage of roquin, derepression of Irf4 as well as T_H17 differentiation correlate to TCR signal strength. Such a 'rheostat' concept of strong antigenic stimulation inducing high Irf4 expression and effector T cell differentiation has recently been shown for $CD8^+$ T cells[40, 41]. One possible scenario how Irf4 levels can determine T_H17 differentiation could involve the graded

transactivation of its target genes such as Hif1α that controls the metabolic pathway of aerobic glycolysis[55], which is likewise required for T_H17 differentiation[42, 43].

Our data involve constitutively expressed roquin-1 and -2 in a cooperation with regnase-1, whose expression can be regulated on the transcriptional, post-transcriptional and post-translational level[1, 10, 11]. Differential expression of these factors may adapt cooperative activity to specific situations and allow differential control of target genes with preferential sensitivities to regnase-1 or roquin. The system also exhibits extensive negative autoregulation, which may prevent desensitization of T cells. Such negative autoregulation includes control of the *Zc3h12a* mRNA by regnase-1 itself[10] as well as by roquin and the potential regulation of CDE sequences present in the 3' UTRs of roquin-1 and roquin-2 encoding mRNAs[7]. Our data show that post-transcriptional repression of *ICOS*, *Ox40*, *Tnf* and *Nfkbiz* mRNAs and T_H17 differentiation in T cells was redundantly controlled by roquin-1 as well as roquin-2 function[7, 8]. Remarkably, very homologous Malt1 cleavage sites were not only present in roquin-1, roquin-2 and regnase-1 but also in regnase-2 and regnase-4 proteins. It is however unknown, whether the cooperation of roquin also extends to redundant functions of other regnase paralogs, and how the regulation of other known and unknown Malt1 targets contributes to T cell fate decisions. Our data provide evidence that Malt1 is activated in a graded manner that is tightly linked to avidity and affinity of the available antigens. The regulation enables a rheostat-like control of roquin and regnase-1 target genes in the T_H17 differentiation pathway and highlights a role for the Malt1 paracaspase in peripheral tolerance and the development of autoimmune disease.

ONLINE METHODS

Mice.

C57BL/6 and BALB/cJ-Tg(DO11.10)10Dlo; Tg(CARΔ-1) mice were obtained from Taconic Farms, and NOD.Cg-*Prkdc*^{scid} *Il2rg*^{tm1Wjl}/SzJ as well as MRL$^{lpr/lpr}$ mice were purchased from Jackson laboratory. *Rc3h1*^{san} mice (EM:02168) were obtained from EMMA consortia. TCR-transgenic Smarta Tg(TcrLCMV)Aox[44], and OT-II mice Tg(TcraTcrb)425Cbn[45], *Malt1*$^{-/-}$[14], *Rc3h1*$^{fl/fl}$[25], *Rc3h2*$^{fl/fl}$[8], *CAG-CAR*$^{stop\text{-}fl}$[8] (K. Heger and M. Schmidt-Supprian unpublished), *Cd4-cre*[46] and compound mutant mice were maintained on a C57BL/6 genetic background. All animals were housed in a pathogen-free barrier facility in accordance with the Helmholtz Zentrum München, Ludwig-Maximilians-University München, Technical University München and institutional, state and federal guidelines.

Generation of overexpression and knockdown vectors.

As a reporter-gene, the human ICOS (ICOS) coding sequence (CDS) was cloned into the pCR8/GW/TOPO vector (Life Technologies) and sequences of the 3' UTRs from *cRel* (1-537), *Ctla4* (1-1090), *Nfkbid* (1-559), *Nfkbiz* (1-1333), *Il6* (1-403), *Irf4* (1-3260) and *Tnf* (490-749; the CDE260 element) were ligated downstream of it into an *XhoI* site. The reporter-3' UTR-sequence was then transferred into the KMV-IRES-GFP retroviral vector using Gateway recombination (Life Technologies). Roquin-1, regnase-1, cre or hMALT1 expression constructs were generated by integrating each of these CDS into the MSCV-IRES-Thy1.1 expression vector. Any mutants thereof were generated using site-directed mutagenesis (QuikChange II, Agilent) with primers from Metabion (Munich). For roquin-1-P2A-mcherry and regnase-1-P2A-mcherry expression vectors the roquin-1 or regnase-1 open reading frame was fused without Stop codon to a P2A-sequence and the mcherry fluorescent protein open reading frame. Adenoviral shRNAs against IκBζ (*Nfkbiz1* CAGCACCTCATTGTGCAAGAT or *Nfkbiz2* GCGTCAATGTACCAGTATTCG), against IκBNS (*Nfkbid1* CAGCTGGATATTCGTGAACAT or *Nfkbid2*

GCCAGGAGATCAAGAGCAACA), and against regnase-1 (*Zc3h12a* AGCGAGGCCACACAGATATTA) were purchased from Sirion Biotech.

Origin of antibodies, peptides and reagents.

Hybridomas and monoclonal antibodies against roquin-1 and roquin-2 (anti-roquin, clone 3F12) and anti-CD3 (145-2C11), anti-CD28 (37N), anti-IL-12 (C17.8), anti-IL-4 (11B11), anti-IFN-γ (Xmg1.2) anti-CD16/32 (2.4G2) were previously described[8] and produced in house. Monoclonal anti-regnase-1 antibody (15D11) was generated by injecting rat with recombinant full-length regnase-1 protein. Polyclonal anti-roquin-1 antibody (#A300-514A) was purchased from Bethyl laboratories, anti-c-Rel (B-6), anti-MALT1 (B12), anti-Cyld (E10) and anti-tubulin (B-5-1-2) were obtained from Santa Cruz Biotech. Anti-Irf4 (P173) was obtained from Cell Signaling. Monoclonal anti-MCPIP-1/ Zc3h12a/ regnase-1 (604421) was purchased from R&D Systems and anti-Thy1.1 (Ox7), anti-CCR6 (140706), recombinant mouse IL-12, as well as anti-RORγt (Q31-378) from BD Pharmingen. Anti-IκBζ (LK2NAP), anti-mouse/-rat Thy1.1 (clone HIS51), anti-hICOS (clone ISA-3), anti-Gr-1 (RB6-8C5), anti-F4/80 (BM8), anti-IFNγ (XMG1.2), anti-IL-17A (eBio17B7), anti-IL-4 (11B11), anti-Foxp3 (FJK16s), anti-CD4 (GK1.5) as well as streptavidin-PE were obtained from eBioscience. Anti-mIL-2 (JES6-5H4) was purchased from Miltenyi Biotec. Recombinant mouse IL-4, IL-6 or human TGFβ were purchased from R&D systems, recombinant hIL-2 (ProleukinS) from Novartis. Rabbit anti-IκBNS antibodies were previously described[36]. Anti-GAPDH (6C5), phorbol-12-myristate-13-actetate (PMA), ionomycin and MG132 were purchased from Calbiochem. Antibodies for immunohistochemistry against CD3 and Ki67 were purchased from NeoMarkers. MHC Class II antibody (EPR1394Y) was purchased from Novus Biologicals. Anti-CD45 and anti-phospho-STAT3 were purchased from BD Bioscience and Cell Signaling, respectively. LCMV glycoprotein gp_{61-80} and $OVA_{323-339}$ WT (ISQAVHAA**H**AEINEAGR), R9

(ISQAVHAA**R**AEINEAGR) and F9 (ISQAVHAA**F**AEINEAGR) peptides were purchased from Biotrend. Thioridazine hydrochloride, Leupeptin, collagenase IV and Brefeldin A were purchased from Sigma-Aldrich and Mepazine acetate from Chembridge. DNaseI was purchased from Roche and Ac-DEVD-CHO as well as zVRPR-fmk were purchased from Enzo Life Sciences or Alexis Biochemicals.

Histopathological evaluation.

Paraformaldehyde (4 %) fixed and paraffin-embedded lung, stomach, small intestine, skin tissues were cut as 2 µm thick sections. For joint preparation, hind legs were fixed in 4 % paraformaldehyde for 1 day, followed by 2 weeks of decalcification in 12.5 % EDTA (pH 7.4) on a horizontal shaker in slow motion. Then the legs were paraffin embedded and cut for stainings. The tissues were stained with Hematoxylin/Eosin or various primary and secondary antibodies in Bond primary antibody diluent (Leica). The staining was performed on a BOND-MAX immunohistochemistry robot (Leica Biosystems) using BOND polymer refine detection solution for DAB. Image acquisition was performed with a Leica SCN400 slide scanner. Alcian blue Peroxide Acid Schiff (Ab-PAS) staining for Goblet cells and Elastica van Gieson staining for pulmonary arteries was performed by incubating paraffin-embedded lung tissue in Ventana buffer. Staining was performed on a NEXES immuno-histochemistry robot (Ventana Instruments) using an IVIEW DAB Detection Kit (Ventana). The numbers of cells positive for the different markers were determined using SlidePath TissueIA image analysis software (Leica) on whole paraffin embedded tissue sections and normalized to tissue area. $CD45^+$, $Ki67^+$, p-$STAT3^+$ or $CD3^+$ cells on paraffin-embedded lung, stomach, skin or intestine sections were counted automatically. Tissue areas positively stained for MHC class II were quantified numerically (positive cells per total cells) or densitometrically (area stained per total area) and normalized to the total tissue area. Pictures for representation

were taken by scanning whole tissue sections using Leica SCN400 slide scanner. For quantification of Goblet cells positively stained for Ab-PAS, four different areas were randomly selected and analyzed in a blinded fashion (positive cells per bronchial epithelial cell area) using a SCN400 slide scanner analysis software (Leica). Representative pictures of Elastica van Gieson stainings were taken and measured on an Olympus Microscope BX53 and a DP72 camera together with the 'cellSens' software (Olympus).

Cell isolation, culture and stimulation.

HEK293T and 293A cells were obtained from ATCC and Invitrogen, respectively. MEF cell lines for *Rc3h1-2*$^{-/-}$, *Rc3h1-2*$^{fl/fl}$*; Cre-ERT2*, *Malt1*$^{-/-}$ and *Zc3h12a*$^{-/-}$ were prepared and grown as previously described[8, 13, 47]. For single cell suspensions lungs were perfused with 10 ml PBS through the right ventricle, cut into small pieces, and digested for 1 h at 37 °C in RPMI containing 4 mg/ml collagenase IV, 20 µg/ml DNaseI, and 10 % FBS. Predigested lung tissue or intact spleens or lymph nodes were homogenized in a cell strainer. The solution was sieved through 70 µm fine mesh. For lamina propria cell preparation from intestine, Peyer's Patches were carefully removed, and the intestine segments were longitudinal opened, washed in ice-cold PBS, and cut into small pieces. The fragments were shaken for 20 min at RT in PBS supplemented with 1 % FCS, 1 mM DTT, 1.35 mM EDTA, then shaken for 40 min at RT in the same media without DTT. After washing in PBS, the remaining tissues were digested for 1 h at 37 °C in RPMI containing 0.4 mg/ml collagenase IV. Single cell suspensions were used for further analysis. If required, $CD4^+$ T cells were enriched by Dynabeads (Invitrogen) positive selection according to the manufacturers' instructions, or FACS-sorted for naive T cell population as $CD4^+CD62L^+CD44^-$ on an Aria III (BD) device. T cells were cultured in RPMI supplemented with 10 % (vol/vol) FBS, 1 x nonessential amino acids, 1 mM sodium-

pyruvate (Lonza), 10 mM HEPES pH 7.4, 1 x eagle MEM essential vitamin mixture (Lonza), 2 mM L-glutamine (Invitrogen), 50 µM β-mercaptoethanol (Sigma) and 100 U/ml penicillin-streptomycin (Invitrogen). Dynabeads-selected $CD4^+$ T cells were stimulated with anti-CD3 (0.25 µg/ml) and anti-CD28 (2.5 µg/ml) on goat anti-hamster IgG (MP Biochemicals) pre-coated 6-well plates. The blasts were expanded by addition of recombinant hIL-2 (20 U/ml, ProleukinS, Novartis). For differentiation, naive $CD4^+$ T cells were cultured in 96-well plates pre-coated with anti-CD3 (1 µg/ml) and anti-CD28 (10 µg/ml) in different culture conditions with the following cytokines and antibodies. T_H1: IL-12 (10 ng/ml) and anti-IL-4 (10 µg/ml). T_H2: IL-4 (20 ng/ml), anti-IL-12 (10 µg/ml), anti-IFNγ (5 µg/ml) and IL-2 (20 U/ml). T_H17: TGFβ (10 ng/ml), IL-6 (60 ng/ml), anti-IL-12 (10 µg/ml), anti-IL-4 (10 µg/ml), anti- IFN-γ (5 µg/ml) and anti-IL-2 (2.5 µg/ml). Treg: TGFβ (10 ng/ml), IL-2 (100 U/ml). T_H1, T_H17 and Treg cells were cultured for 3 d and T_H2 cells were cultured for 5 days. For restimulation cells were washed twice with PBS and incubated for 4 h with PMA (20 nM) and ionomycin (1 µM) in the presence of Brefeldin A (10 µg/ml) 2 h before intracellular staining of cytokines. Peripheral Blood Mononuclear Cells (PBMCs) were obtained by density centrifugation on Pancoll human (Pan Biotech, density 1,077 g/l). Human naive $CD4^+$ T cells were MACS-sorted using the Naive $CD4^+$ T Cell Isolation Kit II (Miltenyi Biotec) according to the manufacturers' instructions and further cultured in Aim-V (Invitrogen) supplemented with 10 % (vol/vol) human pooled serum, 50 µg/ml gentamycin, 2 mM L-glutamine and 10 mM HEPES pH 7.4. APCs were prepared from spleen and lymph node cells of wild-type mice, irradiated (2000 rad) and subsequently pulsed for 1 h at 37 °C with 5 µg/mL LCMV glycoprotein gp_{61-80} or 0.1 - 10 µg/mL $OVA_{323-339}$ peptide WT, R9 or F9 (high to low affinity). APCs were washed twice for short-term stimulation (18 h) experiments to remove excess peptide or not washed for differentiation experiments before being plated with purified Smarta or OTII $CD4^+$ T cells in a ratio of 10:1.

Protein purification and MALT1 *in vitro* cleavage reaction.

Full-length roquin-1 was expressed from a construct containing an amino-terminal His_6-tag and a carboxy-terminal Strep-tag II in the *E. coli* strain Rosetta2 (DE3). The protein was purified using two consecutive affinity chromatography steps on a HiTrap chelating (GE Healthcare) and a StrepTrap column (GE Healthcare). The purification buffer was 50 mM Tris-HCl pH 8.0, 300 mM NaCl, and 0.01 % (vol/vol) 1-thioglycerol. GST-MALT1 was produced in BL21 Codonplus RILP bacteria after induction with 50 µM IPTG at 18 °C over night. The proteins were purified from bacterial lysate via an Äkta liquid chromatography system as described[28]. Recombinant full-length roquin-1 (5 µg) was incubated with human recombinant full-length GST-MALT1 (5 µg) in the presence or absence of the MALT1 peptide inhibitor z-VRPR-fmk (5 µM) for 1 h at 30 °C in 50 µl cleavage buffer (50 mM MES, pH 7.0; 150 mM NaCl; 10 % (w/vol) saccharose; 0.1 % (w/vol) CHAPS; 1M sodium citrate; 10 mM DTT).

Virus production and cell transduction.

Replication-deficient retrovirus or adenovirus and MEF or T cell transduction was performed as previously described[6, 8, 48].

Protein detection by immunoblotting.

$CD4^+$ T or MEF cells were incubated for 15 min on ice with lysis buffer (20 mM Tris-HCl, pH 7.5, 150 mM NaCl, 0.25 % [vol/vol] Nonidet-P40, 1.5 mM $MgCl_2$, protease inhibitor mix without EDTA (Roche) and 1 mM DTT). After mixing the lysate was cleared by centrifugation (10 min, 10000 g, 4 °C). The protein content in the lysate was determined using BioRad Protein assay. For immunoblotting 50-70 µg of total protein were loaded per lane and detection was performed according to standard protocols. Lung and pancreas tissue lysates were prepared from NOD.Cg-*Prkdc*^{scid} *Il2rg*^{tm1Wjl}/SzJ mice**.** Organs were lysed (20 mM Tris-HCl, pH 7.5, 150 mM NaCl, 0.25

%(vol/vol) Nonidet-P40, 1.5 mM $MgCl_2$, 1 mM EDTA, and protease inhibitor mix without EDTA) on ice, shock frozen, thawed again and centrifuged (10 min, 10000 g, 4 °C). Supernatants were then collected for immunoblot analysis. 25 µg of lung or pancreas protein extract per lane were loaded on an SDS-PAGE (10 % polyacrylamide). Blots were probed over night at 4 °C with individual mouse sera diluted 1:200 in 5 % BSA and subsequently incubated with anti-mouse IgG HRP followed by ECL detection.

Mouse serum preparation and ELISA for cytokine and autoantibody detection.

To prepare mouse sera for immunoblot and ELISA, mice were sacrificed and blood was drawn from the heart, incubated on ice for 3 h and centrifuged for 10 min at 13.000 g to yield the supernatant. Autoantibody levels were determined by ELISA as described[49]. To detect anti-dsDNA antibodies NUNC maxisorp ELISA plates were coated with poly-L-lysine (Trevigen, Gaithersburg, MD, USA) and mouse embryonic stem cell dsDNA. After incubation with mouse serum, dsDNA-specific IgG levels were detected by ELISA (Bethyl Labs, Montgomery, TX, USA). Rheumatoid factor: ELISA plates were coated with 10 µg/ml rabbit IgG (Jackson Immunoresearch, West Grove, PA, USA) overnight at 4°C. Serum samples were diluted 1:10, HRP conjugated anti-mouse IgG was used as secondary antibody. To detect IFN-γ, IL-17A, IL-6, IL-10 and TNF cytokine levels, ELISA kits from eBioscience were used following the manufacturer's instructions. Absorbance was measured at 450 nm with a Sun-rise plate reader (TECAN) and concentrations were calculated according to the standard curve.

Flow cytometry and intracellular staining.

Single cell suspensions were pre-incubated with Fc-block (CD16/32) in staining buffer (PBS with 2 % FBS and 2 mM EDTA) for 10 min at 4 °C and stained with

antibodies for 20 min at 4 °C. For intracellular cytokine stainings isolated $CD4^+$ T cells were stimulated for 4 h with PMA (20 nM) and ionomycin (1 µM) and for the last 2 h Brefeldin A (10 ng/ml; Sigma) was added. Then fixable dead cell staining (Invitrogen) was performed for 30 min at 4 °C, followed by surface staining. Cells were fixed with 4 % paraformaldehyde (MERCK) for 10 min at room temperature and permeabilized for 20 min at 4 °C in PBS containing 0.5 % saponin (VWR international) and 1 % BSA (ROTH). The cells were then stained with anti-cytokine antibodies for 50 min at 4 °C. To stain for transcription factors, unstimulated cells were fixed with fixation/permeabilization buffer for 1 h at 4 °C, then incubated in permeabilization buffer for 20 min at 4 °C (according to the Foxp3 staining kit from eBioscience) and finally stained with anti-transcription factor antibodies. Cells were acquired on an LSR Fortessa (BD) device and samples were analyzed with FlowJo software (Tree Star).

Statistical analysis.

Statistical analyses were performed with GraphPad Prism 5.0d and p-values were calculated by Student's t-test, one-way analysis of variance (ANOVA) with Tukey's multiple comparisons test.

ACKNOWLEDGEMENTS

We thank H.-M. Jäck and J. Wittmann (Friedrich-Alexander-Universität Erlangen, Germany) for the kind gift of the cloned 3' UTR of mouse Irf4. This work received support from an ERC grant to V.H. and the DFG SFB1054 collaborative research grants to V.H., J.R. D.K. M.S-S. (TP-A03, Z02, B01, A04 and A02). M.H. was supported by the SFB TR36, an ERC grant, the PCCC and the Hofschneider foundation. H.-J.A and M.L. were supported by DFG GRK1202 and H.H. was

supported by DFG HO1116/5-2. G.A.H or K.U.V were supported by a fellowship from the Boehringer Ingelheim Fonds or FEBS, respectively. We thank Dirk Baumjohann for critical reading of the manuscript.

AUTHOR CONTRIBUTIONS

D.H., K.M.J. and S.B did most of the experiments with J.Z., G.A.H., D.N., K.U.V., N. R., S.C.W., S.L.E., N.M., C.L., J.S., R.G, A.K. and L.M. contributing specific experiments. V.H. conceived the project, designed the experiments and wrote the paper together with D.H., K.M.J and S.B. Unpublished reagents or reagents and advice as well as additional design and supervision of experiments was provided by A.G., A.W., H-J.A., I.S., M.S-S., M.F., H.H., D.K, J.R. and M.H.

COMPETING FINANCIAL INTERESTS

The authors declare no competing financial interests.

REFERENCES

1. Matsushita K, Takeuchi O, Standley DM, Kumagai Y, Kawagoe T, Miyake T*, et al.* Zc3h12a is an RNase essential for controlling immune responses by regulating mRNA decay. *Nature* 2009, **458**(7242)**:** 1185-1190.

2. Miao R, Huang S, Zhou Z, Quinn T, Van Treeck B, Nayyar T*, et al.* Targeted disruption of MCPIP1/Zc3h12a results in fatal inflammatory disease. *Immunology and cell biology* 2013, **91**(5)**:** 368-376.

3. Vinuesa CG, Cook MC, Angelucci C, Athanasopoulos V, Rui L, Hill KM*, et al.* A RING-type ubiquitin ligase family member required to repress follicular helper T cells and autoimmunity. *Nature* 2005, **435**(7041)**:** 452-458.

4. Zhou Z, Miao R, Huang S, Elder B, Quinn T, Papasian CJ*, et al.* MCPIP1 deficiency in mice results in severe anemia related to autoimmune mechanisms. *PloS one* 2013, **8**(12)**:** e82542.

5. Ivanov P, Anderson P. Post-transcriptional regulatory networks in immunity. *Immunological reviews* 2013, **253**(1)**:** 253-272.

6. Glasmacher E, Hoefig KP, Vogel KU, Rath N, Du L, Wolf C*, et al.* Roquin binds inducible costimulator mRNA and effectors of mRNA decay to induce microRNA-independent post-transcriptional repression. *Nature immunology* 2010, **11**(8)**:** 725-733.

7. Leppek K, Schott J, Reitter S, Poetz F, Hammond MC, Stoecklin G. Roquin promotes constitutive mRNA decay via a conserved class of stem-loop recognition motifs. *Cell* 2013, **153**(4)**:** 869-881.

8. Vogel KU, Edelmann SL, Jeltsch KM, Bertossi A, Heger K, Heinz GA*, et al.* Roquin paralogs 1 and 2 redundantly repress the Icos and Ox40 costimulator mRNAs and control follicular helper T cell differentiation. *Immunity* 2013, **38**(4)**:** 655-668.

9. Yu D, Tan AH, Hu X, Athanasopoulos V, Simpson N, Silva DG*, et al.* Roquin represses autoimmunity by limiting inducible T-cell co-stimulator messenger RNA. *Nature* 2007, **450**(7167)**:** 299-303.

10. Iwasaki H, Takeuchi O, Teraguchi S, Matsushita K, Uehata T, Kuniyoshi K*, et al.* The IkappaB kinase complex regulates the stability of cytokine-encoding mRNA induced by TLR-IL-1R by controlling degradation of regnase-1. *Nature immunology* 2011, **12**(12)**:** 1167-1175.

11. Uehata T, Iwasaki H, Vandenbon A, Matsushita K, Hernandez-Cuellar E, Kuniyoshi K*, et al.* Malt1-induced cleavage of regnase-1 in CD4(+) helper T cells regulates immune activation. *Cell* 2013, **153**(5)**:** 1036-1049.

12. Suzuki HI, Arase M, Matsuyama H, Choi YL, Ueno T, Mano H*, et al.* MCPIP1 ribonuclease antagonizes dicer and terminates microRNA biogenesis through precursor microRNA degradation. *Molecular cell* 2011, **44**(3)**:** 424-436.

13. Schlundt A, Heinz GA, Janowski R, Geerlof A, Stehle R, Heissmeyer V*, et al.* Structural basis for RNA recognition in roquin-mediated post-transcriptional gene regulation. *Nature structural & molecular biology* 2014.

14. Tan D, Zhou M, Kiledjian M, Tong L. The ROQ domain of Roquin recognizes mRNA constitutive-decay element and double-stranded RNA. *Nature structural & molecular biology* 2014.

15. Coornaert B, Baens M, Heyninck K, Bekaert T, Haegman M, Staal J*, et al.* T cell antigen receptor stimulation induces MALT1 paracaspase-mediated cleavage of the NF-kappaB inhibitor A20. *Nature immunology* 2008, **9**(3)**:** 263-271.

16. Rebeaud F, Hailfinger S, Posevitz-Fejfar A, Tapernoux M, Moser R, Rueda D*, et al.* The proteolytic activity of the paracaspase MALT1 is key in T cell activation. *Nature immunology* 2008, **9**(3)**:** 272-281.

17. Thome M. Multifunctional roles for MALT1 in T-cell activation. *Nature reviews Immunology* 2008, **8**(7)**:** 495-500.

18. Duwel M, Welteke V, Oeckinghaus A, Baens M, Kloo B, Ferch U*, et al.* A20 negatively regulates T cell receptor signaling to NF-kappaB by cleaving Malt1 ubiquitin chains. *Journal of immunology* 2009, **182**(12)**:** 7718-7728.

19. Hailfinger S, Nogai H, Pelzer C, Jaworski M, Cabalzar K, Charton JE*, et al.* Malt1-dependent RelB cleavage promotes canonical NF-kappaB activation in lymphocytes and lymphoma cell lines. *Proceedings of the National Academy of Sciences of the United States of America* 2011, **108**(35)**:** 14596-14601.

20. Staal J, Driege Y, Bekaert T, Demeyer A, Muyllaert D, Van Damme P*, et al.* T-cell receptor-induced JNK activation requires proteolytic inactivation of CYLD by MALT1. *The EMBO journal* 2011, **30**(9)**:** 1742-1752.

21. Brustle A, Brenner D, Knobbe CB, Lang PA, Virtanen C, Hershenfield BM*, et al.* The NF-kappaB regulator MALT1 determines the encephalitogenic potential of Th17 cells. *The Journal of clinical investigation* 2012, **122**(12)**:** 4698-4709.

22. Gringhuis SI, Wevers BA, Kaptein TM, van Capel TM, Theelen B, Boekhout T*, et al.* Selective C-Rel activation via Malt1 controls anti-fungal T(H)-17 immunity by dectin-1 and dectin-2. *PLoS pathogens* 2011, **7**(1)**:** e1001259.

23. Mc Guire C, Wieghofer P, Elton L, Muylaert D, Prinz M, Beyaert R*, et al.* Paracaspase MALT1 deficiency protects mice from autoimmune-mediated demyelination. *Journal of immunology* 2013, **190**(6)**:** 2896-2903.

24. Mc Guire C, Elton L, Wieghofer P, Staal J, Voet S, Demeyer A*, et al.* Pharmacological inhibition of MALT1 protease activity protects mice in a mouse model of multiple sclerosis. *Journal of neuroinflammation* 2014, **11**(1)**:** 124.

25. Bertossi A, Aichinger M, Sansonetti P, Lech M, Neff F, Pal M*, et al.* Loss of Roquin induces early death and immune deregulation but not autoimmunity. *The Journal of experimental medicine* 2011, **208**(9)**:** 1749-1756.

26. Cohen PL, Eisenberg RA. Lpr and gld: single gene models of systemic autoimmunity and lymphoproliferative disease. *Annual review of immunology* 1991, **9:** 243-269.

27. Lee SK, Silva DG, Martin JL, Pratama A, Hu X, Chang PP*, et al.* Interferon-gamma excess leads to pathogenic accumulation of follicular helper T cells and germinal centers. *Immunity* 2012, **37**(5)**:** 880-892.

28. Nagel D, Spranger S, Vincendeau M, Grau M, Raffegerst S, Kloo B*, et al.* Pharmacologic inhibition of MALT1 protease by phenothiazines as a therapeutic approach for the treatment of aggressive ABC-DLBCL. *Cancer cell* 2012, **22**(6)**:** 825-837.

29. Wiesmann C, Leder L, Blank J, Bernardi A, Melkko S, Decock A*, et al.* Structural determinants of MALT1 protease activity. *Journal of molecular biology* 2012, **419**(1-2)**:** 4-21.

30. Liang J, Saad Y, Lei T, Wang J, Qi D, Yang Q*, et al.* MCP-induced protein 1 deubiquitinates TRAF proteins and negatively regulates JNK and NF-kappaB signaling. *The Journal of experimental medicine* 2010, **207**(13)**:** 2959-2973.

31. Okamoto K, Iwai Y, Oh-Hora M, Yamamoto M, Morio T, Aoki K*, et al.* IkappaBzeta regulates T(H)17 development by cooperating with ROR nuclear receptors. *Nature* 2010, **464**(7293)**:** 1381-1385.

32. Robertson JM, Jensen PE, Evavold BD. DO11.10 and OT-II T cells recognize a C-terminal ovalbumin 323-339 epitope. *Journal of immunology* 2000, **164**(9)**:** 4706-4712.

33. Fogli LK, Sundrud MS, Goel S, Bajwa S, Jensen K, Derudder E*, et al.* T cell-derived IL-17 mediates epithelial changes in the airway and drives pulmonary neutrophilia. *Journal of immunology* 2013, **191**(6)**:** 3100-3111.

34. Korn T, Mitsdoerffer M, Croxford AL, Awasthi A, Dardalhon VA, Galileos G*, et al.* IL-6 controls Th17 immunity in vivo by inhibiting the conversion of conventional T cells into Foxp3+ regulatory T cells. *Proceedings of the National Academy of Sciences of the United States of America* 2008, **105**(47)**:** 18460-18465.

35. Bauquet AT, Jin H, Paterson AM, Mitsdoerffer M, Ho IC, Sharpe AH*, et al.* The costimulatory molecule ICOS regulates the expression of c-Maf and IL-21 in the development of follicular T helper cells and TH-17 cells. *Nature immunology* 2009, **10**(2)**:** 167-175.

36. Schuster M, Glauben R, Plaza-Sirvent C, Schreiber L, Annemann M, Floess S*, et al.* IkappaB(NS) protein mediates regulatory T cell development via induction of the Foxp3 transcription factor. *Immunity* 2012, **37**(6)**:** 998-1008.

37. Chen G, Hardy K, Pagler E, Ma L, Lee S, Gerondakis S*, et al.* The NF-kappaB transcription factor c-Rel is required for Th17 effector cell development in experimental autoimmune encephalomyelitis. *Journal of immunology* 2011, **187**(9)**:** 4483-4491.

38. Reinhard K, Huber M, Wostl C, Hellhund A, Toboldt A, Abass E*, et al.* c-Rel promotes type 1 and type 17 immune responses during Leishmania major infection. *European journal of immunology* 2011, **41**(5)**:** 1388-1398.

39. Ruan Q, Kameswaran V, Zhang Y, Zheng S, Sun J, Wang J*, et al.* The Th17 immune response is controlled by the Rel-RORgamma-RORgamma T transcriptional axis. *The Journal of experimental medicine* 2011, **208**(11)**:** 2321-2333.

40. Man K, Miasari M, Shi W, Xin A, Henstridge DC, Preston S*, et al.* The transcription factor IRF4 is essential for TCR affinity-mediated metabolic programming and clonal expansion of T cells. *Nature immunology* 2013, **14**(11)**:** 1155-1165.

41. Yao S, Buzo BF, Pham D, Jiang L, Taparowsky EJ, Kaplan MH*, et al.* Interferon regulatory factor 4 sustains CD8(+) T cell expansion and effector differentiation. *Immunity* 2013, **39**(5)**:** 833-845.

42. Dang EV, Barbi J, Yang HY, Jinasena D, Yu H, Zheng Y*, et al.* Control of T(H)17/T(reg) balance by hypoxia-inducible factor 1. *Cell* 2011, **146**(5)**:** 772-784.

43. Shi LZ, Wang R, Huang G, Vogel P, Neale G, Green DR*, et al.* HIF1alpha-dependent glycolytic pathway orchestrates a metabolic checkpoint for the differentiation of TH17 and Treg cells. *The Journal of experimental medicine* 2011, **208**(7)**:** 1367-1376.

44. Oxenius A, Bachmann MF, Zinkernagel RM, Hengartner H. Virus-specific MHC-class II-restricted TCR-transgenic mice: effects on humoral and cellular immune responses after viral infection. *European journal of immunology* 1998, **28**(1)**:** 390-400.

45. Barnden MJ, Allison J, Heath WR, Carbone FR. Defective TCR expression in transgenic mice constructed using cDNA-based alpha- and beta-chain genes under the control of heterologous regulatory elements. *Immunology and cell biology* 1998, **76**(1)**:** 34-40.

46. Lee PP, Fitzpatrick DR, Beard C, Jessup HK, Lehar S, Makar KW*, et al.* A critical role for Dnmt1 and DNA methylation in T cell development, function, and survival. *Immunity* 2001, **15**(5)**:** 763-774.

47. Ansel KM, Pastor WA, Rath N, Lapan AD, Glasmacher E, Wolf C*, et al.* Mouse Eri1 interacts with the ribosome and catalyzes 5.8S rRNA processing. *Nature structural & molecular biology* 2008, **15**(5)**:** 523-530.

48. Warth SC, Heissmeyer V. Adenoviral transduction of naive CD4 T cells to study treg differentiation. *Journal of visualized experiments : JoVE* 2013(78).

49. Lech M, Kulkarni OP, Pfeiffer S, Savarese E, Krug A, Garlanda C*, et al.* Tir8/Sigirr prevents murine lupus by suppressing the immunostimulatory effects of lupus autoantigens. *The Journal of experimental medicine* 2008, **205**(8)**:** 1879-1888.

FIGURE LEGENDS

Figure 1 Comparison of inflammatory phenotypes in the lung of roquin mutant mice. (**a**) Histological sections of H&E-stained lung tissue from *Rc3h1-2$^{fl/fl}$; Cd4-cre* mice and littermate WT controls at the indicated ages (magnification 20x, scale bars represent 100 µm in overview of upper and middle panels and 10 µm in zoomed sections of the lower panel). (**b**) Histological sections of H&E stained alveoli (magnification 20x, scale bar represents 100 µm for left and middle panels, magnification 40x and scale bar represents 10 µm for right panel), anti-CD3-, anti-MHC II- and anti-Ki67-stained lung tissues of representative 18-23 weeks old mice (40x magnification, for left and middle panel, and 80x for right panel, scale bar represent 10 µm). (**c**) Quantification of $CD3^+$, MHC II^+ and $Ki67^+$ cells in lung tissue. (**d**) Alcian blue (Ab) periodic acid-Schiff (PAS) stained goblet cells in bronchioles of *Rc3h1-2$^{fl/fl}$; Cd4-cre* and WT control mice. Arrowheads indicate exemplary positive

cells (magnification 40x, scale bar represents 10 µm). (**e**) Quantification of Ab-PAS$^+$ goblet cells. (**f**) Elastica van Gieson stain of small and large arteries. Arrowheads indicate diameter measurements (magnification 60x, Scale bars represent 1mm). Data represent analyses of 3 WT and 4 *Rc3h1-2$^{fl/fl}$; CD4-cre* mice (**a-f**) Error bars are mean ± SEM * P<0.05. ** P<0.01 (unpaired, two-tailed t test). (**g–h**) Immunoblots of lung tissue (**g**) or pancreas tissue (**h**) protein extracts from immune deficient NOD/Scid/cγ$^{-/}$mice. Immunoblots were probed with sera from MRL$^{lpr/lpr}$, control WT*; Cd4-cre*, *Rc3h1-2$^{fl/fl}$; Cd4-cre* and *Rc3h1$^{san/san}$* mice that were selected to equally represent individuals of both sexes at an age of 10-23 weeks with the weakest, the strongest as well as with intermediate reactivities as determined by pretesting of a larger cohort using lung tissue antigen immunoblots.

Figure 2 Enhanced T_H17 differentiation and gastritis in mice that lack roquin in T cells. IL-17A (**a**), IL-6 (**b**), TNF (**c**), IL-10 (**d**) and IFN-γ (**e**) concentrations in the sera of 12-18 weeks old WT*; Cd4-cre* and *Rc3h1-2$^{fl/fl}$*; *Cd4-cre* mice as determined by ELISA. Sera from wild-type and roquin mutant genotypes were used from 4/5 (**a-b**), 10/10 (**c**), 11/11 (**d**), 4/4 (**e**) mice to perform ELISAs. FACS-analyses of IL-17A versus IFN-γ in PMA and ionomycin-stimulated CD4$^+$ T cells from lymph node and lung **(f)** and of neutrophils (Gr-1^{hi}F4/80$^-$) in the lung **(g)** of 12-18 weeks old WT*; Cd4-cre* and *Rc3h1-2$^{fl/fl}$*; *Cd4-cre* mice. Contour blots are representative of 7 (**f**) or 3 (**g**) independent experiments with one mouse per genotype. (**h–k**) *In vitro* differentiation of naive CD4$^+$CD62L$^+$CD44$^-$ T cells from WT*; Cd4-cre* or *Rc3h1-2$^{fl/fl}$*; *Cd4-cre* mice cultured under T_H17 (**h**), Treg (**i**), T_H1 (**j,** upper panel) or T_H0 (**j**, lower panel) or T_H2 (**k**) conditions. Cells were restimulated and intracellularly stained for the indicated cytokines IL-17A, IFN-γ, IL-4 (**h, j, k**) or for the transcription factor Foxp3 (**i**). Data in (**h-j**) or (**k**) are representative of 3 or 2 independent experiments, respectively. (**l**) Stomach sections stained for H&E, anti-CD3, anti-CD45 and anti-p-STAT3.

Representatives of six technical replicates from three 26-30 weeks old WT*; Cd4-cre* or *Rc3h1-2*$^{fl/fl}$; *Cd4-cre* mice are shown (20x magnification, scale bar represents 100 µm), and CD3$^+$, CD45$^+$ and p-STAT3$^+$ cells are quantified **(m)**. Error bars are mean ± SEM with the indicated p-values, * P<0.05, ** P<0.01, *** P<0.001 (unpaired, two-tailed t-test).

Figure 3 Full-length ROQUIN proteins are degraded after antigen and costimulatory receptor triggering. (**a–e**) Immunoblot analyses of ROQUIN expression in CD4$^+$ T cells isolated from wild-type mice (**a**,**d–e**),from the indicated roquin mouse mutants (**b**) or from naive human CD4$^+$ T cells (**c**). CD4$^+$ T cells were left untreated (0) or stimulated for the indicated times with PMA and ionomycin (PMA + iono) (**a–c**), PMA or ionomycin (**d**) or with anti-CD3, anti-CD28 or anti-CD3/anti-CD28 (**e**). In addition, human CD4$^+$ T cells were pretreated with MG132 for 30min (**c**). (**f**) Transgenic CD4$^+$ T cells specific for the LCMV glycoprotein gp_{61-80} from Smarta mice (SMtg) were left unstimulated or cultured with irradiated APCs of WT mice for the indicated times. Prior to co-culture APCs were loaded with 5 µg/ml gp_{61-80} peptide for 1h. Cell extracts were analyzed for roquin protein expression by immunoblots. Arrowheads indicate full-length roquin-1 and -2 proteins; arrowheads with asterisks indicate degradation products. Data are representatives of two (**a–c, f**) or three (**d–e**) independent experiments.

Figure 4 The Malt1 paracaspase cleaves roquin-1 at arginines 510 and 579. (**a**) WT CD4$^+$ T cells were preincubated for 180 min with MG132, Ac-DEVD-CHO or with the Malt1 inhibitors z-VRPR-fmk, Mepazine and Thioridazine. DMSO was included as control. Cells were then stimulated with PMA and ionomycin for 60 min (+) or left untreated (-) and cell extracts were analyzed for roquin protein expression in immunoblots. (**b**) Purified CD4$^+$ T cells from *Malt1*$^{+/-}$ or *Malt1*$^{-/-}$ mice were left untreated (0) or stimulated with PMA and ionomycin for the indicated times and cell

extracts were analyzed for roquin protein expression by immunoblots. (**c–d**) *Malt1*$^{-/-}$ MEF cells were reconstituted with WT MALT1 (**c–d**) or catalytically inactive MALT1 (PM) (**d**). Cells were subsequently infected with retroviruses to express WT roquin-1 or a series of roquin-1 mutants. Cell extracts were then analyzed for roquin protein expression in immunoblots (**c-d**). (**e**) *In vitro* cleavage reactions with recombinant full-length roquin-1 and recombinant GST-MALT1 in the absence or presence of the Malt1 inhibitor z-VRPR-fmk were analyzed by immunoblot of roquin-1. Please note that due to copurification of polypeptides that represent truncated roquin-1, the in vitro cleavage assay also produces faster migrating bands in addition to the main cleavage product. (**f**) CD4^{+} T cells from *Rc3h1*$^{fl/fl}$*; CAG-CAR*$^{stop\text{-}fl}$*; Cd4-cre* mice were reconstituted with roquin-1^{WT}, roquin-1$^{R510G/R579G}$ or roquin-1$^{1\text{-}510}$ expressed from IRES-GFP co-expressing adenoviruses or infected with empty virus. After 3 d of culture under T_H17 conditions, cells were restimulated and stained for Icos expression. Histograms are derived from pregated GFP^{+} cells. (**g**) Alignment of Malt1-dependent cleavage sites in roquin-1 or roquin-2 with cleavage sites of the previously identified Malt1 targets regnase-1, A20, Bcl10, RelB, NIK and Cyld. Arginine residues after which Malt1 cleaves are marked with the respective amino acid position in the target protein. (**h**) T_H17 cells from WT or *Rc3h1-2*$^{fl/fl}$ mice were infected with cre-expressing retroviruses. The cells were rested (0) or restimulated with PMA and ionomycin for 15 or 60 min. Cell extracts were analyzed for expression and cleavage of different Malt1 targets by immunoblot. Data represent two (**b,d,e**) or three (a,**c,f**) independent experiments.

Figure 5 Regnase-1 and roquin-1 regulate a set of shared target mRNAs. (**a**) IL-6 concentrations in the supernatants of roquin- or regnase-1-deficient MEF cells stably transduced with vectors which allowed doxycyclin-inducible expression of roquin-1 or regnase-1 respectively. Cells were cultured for 24 h in medium supplemented with

the depicted combinations of doxycyclin, IL-17A and TNF. Subsequently, IL-6 was detected by ELISA. Each column and error bar represents the mean ± SD from technical triplicates of each culture condition, the data are representative of 2 independent experiments. * P<0.05, ** P<0.01, *** P<0.001 (One way ANOVA with Tukey's test). (**b**) T cell cultures of WT*; CAG-CAR*$^{stop\text{-}fl}$ or *Rc3h1-2*$^{fl/fl}$*; CAG-CAR*$^{stop\text{-}fl}$ mice were transduced with cre-expressing retroviruses to induce the deletion of *Rc3h1* and *Rc3h2* genes. Cell extracts were analyzed for roquin-1 and -2, c-Rel and tubulin expression by immunoblots. (**c**) FACS sorted naive $CD4^+$ T cells from WT; *Cd4-cre* mice (black histograms) and *Rc3h1-2*$^{fl/fl}$; *Cd4-Cre* mice (red histograms) were cultured under T_H17 condition for 48 h. The cells were used for analysis of surface Icos and Ox40 and intracellular Ctla-4 expression. (**d**) MEF cells of the indicated genotypes were tested for protein expression of roquin, regnase-1, IκBNS and tubulin by immunoblots. Please note that due to an unknown modification the specific signals for IκBNS migrate at 35 and 70 kDa[36] (**e–g**). Expression levels of human ICOS as reporter without (*CDS*) or with its natural 3' UTR (*ICOS-3'* UTR) or as fusion with the indicated 3' UTRs of mouse genes in roquin-1-inducible *Rc3h1-2*$^{-/-}$ (**e**), in regnase-1-inducible *Zc3h12a*$^{-/-}$ (**f**) and in *Rc3h1-2*$^{fl/fl}$; *CARstop*^{fl}; *CreERT2* MEF cells. Dotted histograms in **(e-g)** show non-transduced cells, shaded histograms show cells transduced with the reporter and colored histograms show reporter-transduced cells with doxycylin-mediated roquin-1- **(e)** or regnase-1-induction **(g)** or with creERT2-mediated deletion of *Rc3h1-2*$^{fl/fl}$ alleles. Representatives out of two (**a**) or at least three experiments are shown **(b–g)**.

Figure 6 Cooperative regulation of CDE-containing targets by roquin and regnase-1. (**a**) FACS analyses of ICOS-levels in a WT MEF cell clone with stable ICOS expression alone (shaded histogram), with additional doxycyclin-induced roquin-1 overexpression (+ dox; red), with superinfection by regnase-1-IRES-Thy1.1 retrovirus

(+ regnase-1-IRES-Thy1.1; blue) or with both roquin-1-induction and regnase-1-IRES-Thy1.1 overexpression (+ regnase-1-IRES-Thy1.1 / + dox; bold black). (**b-d**) FACS-analyses of *Rc3h1-2*$^{-/-}$ (upper panels) and *Zc3h12a*$^{-/-}$ (lower panels) MEF cells. Cells were transduced with ICOS-CDE260 expressing retrovirus (shaded histograms) and superinfected with roquin-1-IRES-Thy1.1 retrovirus (red histograms) or regnase-1-IRES-Thy1.1 retrovirus (blue histograms) or with mutant forms of these viruses indicated on top of the histogram blots. **(e)** Domain structure of roquin-1 (upper panel), regnase-1 (middle panel) and of a fusion protein consisting of the ROQ-domain and the coding sequence of regnase-1 (bottom panel). The fusion protein consists of the first two codons of endogenous roquin-1 followed by aa131-360, which contain the ROQ-domain. A flexible GSGGRIP-sequence connects the ROQ-domain to regnase-1. **(f)** FACS-analyses of *Rc3h1-2*$^{-/-}$ (upper panel) and *Zc3h12a*$^{-/-}$ (lower panel) MEF cells transduced with ICOS-CDE260 expressing retrovirus (shaded histograms) and superinfected with either roquin-1-IRES-Thy1.1 (red line), regnase-1-IRES-Thy1.1 (blue line) or with retrovirus encoding the fusion protein ROQ-regnase-1-IRES-Thy1.1 (black bold line) as depicted in the bottom panel of **(e)**. All histograms show non-transduced cells by dotted lines and ICOS-expressing cells without roquin-1 or regnase-1 overexpression as shaded lines. Representatives of three or more experiments are shown.

Figure 7 IκBNS and IκBζ promote and regnase-1 inhibits T_H17 differentiation. To knockdown endogenous gene expression $CD4^+$ T cells from Tg(DO11.10); Tg(CARΔ-1) mice (**a-b**) or from WT*; CAG-CAR*$^{stop\text{-}fl}$*; Cd4-cre* or *Rc3h1-2*$^{fl/fl}$*; CAG-CAR*$^{stop\text{-}fl}$*; Cd4-cre* **(c-f**) mice were transduced with adenoviruses encoding for GFP and shRNA against *Zc3h12a* (**a–b, e**), *Nfkbiz* (**a–c**) or *Nfkbid* (**a–b, d**). To ectopically express roquin-1 in its WT or mutant forms, the roquin expression constructs or control (**f**) were adenovirally expressed in naive T cells from *Rc3h1-2*$^{fl/fl}$*; CAG-*

CAR$^{stop\text{-}fl}$*; Cd4-cre* mice. CD4$^+$ T cells were cultured under T_H17 (**a, c-f**) or T_H1-polarizing (**b**) conditions for 3 d, restimulated and stained intracellularly for IL-17A and IFN-γ (**a–f**). Cells are pregated on GFP$^+$**.** Differentiation data are shown as the average after normalization to control transduced cells (**a-b**) or as representatives (**c-f**) of two or more independent experiments.

Figure 8 TCR signal-strength determines derepression of roquin targets. (**a-b**) WT CD4$^+$ T cells were left untreated (0) or stimulated for the indicated times with PMA and ionomycin (**a**) or preincubated for 180 min with DMSO or Mepazine followed by 60 min of PMA and ionomycin stimulation (**b**). Cell extracts were analyzed for roquin-1 and -2, regnase-1, IκBζ, Irf4, IκBNS, tubulin or Gapdh protein expression in immunoblots. (**c-h**) Transgenic OT-II CD4$^+$ T cells specific for the $OVA_{323\text{-}339}$ peptide were unstimulated or cultured with irradiated APCs from WT mice for 16 h (**c-d**) , 24 h (**e-f**) or 72 h (**g-h**). Prior to co-culture APCs were loaded with 0.1 or 1 or 10 µg/ml $OVA_{323\text{-}339}$ WT peptide for 1h (**c, e, g**) or loaded with 10 µg/ml of $OVA_{323\text{-}339}$ peptide WT, R9 or F9 (high to low affinity) (**d, f, h**). Cell extracts were analyzed for roquin and Irf4 protein expression by immunoblots (**c-d**). Irf4 expression levels after 24 h were determined by FACS analysis of CD69$^+$ OT-II cells cultured under T_H17 conditions(**e-f**). The CD4$^+$ T cells were cultured under T_H17 conditions for 3 d, restimulated and intracellularly stained for IL-17A (**g-h**). Arrowheads indicate full-length roquin-1 and -2 proteins; arrowheads with asterisks indicate degradation products. Data are representatives out of two or more experiments (**a-h**).

Supplementary Figure S1 Comparison of inflammatory phenotypes in mice with roquin mutations. (**a**) Histological sections of H&E-stained (magnification 20x, scale bar represents 100 µm) and anti-CD3-, anti-MHCII- and anti-Ki67-stained (magnification 40x, scale bar represents 100 µm) lung tissues from 26-30 weeks old

WT control and *Rc3h1-2$^{fl/fl}$; Cd4-cre* mice. Total numbers of CD45$^+$ (**b**), or relative numbers of CD3$^+$ (**c**), MHC II$^+$ (**d**) and Ki67$^+$ (**e**) cells in lung tissue of 26-30 weeks old WT control and *Rc3h1-2$^{fl/fl}$; Cd4-cre* mice were detected in flow cytometry (**b**) or histology (**c–e**). (**f**) Kaplan-Meier survival curve of *Rc3h1-2$^{fl/fl}$; Cd4-cre* mice. (**g–h**) Anti-DNA antibodies (**g**) and rheumatoid factor (**h**) in sera from WT*; Cd4-cre*, from *Rc3h1-2$^{fl/fl}$; Cd4-cre* and from *Rc3h1$^{san/san}$* mice were detectd by ELISA. Results represent analyses of 5/5 (**a, c-e**), 9/7 (**b**), 4/5/5 (**g,h**) wild-type and mutant mice. Statistically significant differences are indicated by asterisks, error bars are mean ± SEM (**b-e**), or mean ± SD (**g-h**) (unpaired, two-tailed t-test for **b-e**, One way ANOVA with Tukey's test for **g,h**). * P<0.05. ** P<0.01. *** P<0.001.

Supplementary Figure S2 Lack of roquin in T cells does not induce inflammation in skin, intestine and joint. (**a-c**) Lung CD4$^+$ cells (**a-b**) or CD45$^+$ cells (**c**) from 12-18 weeks old WT*; Cd4-cre* and *Rc3h1-2$^{fl/fl}$*; *Cd4-cre* mice were used for CD4 versus IL-4 (**a**), or RORγt (**b**) stainings or for IL-17A versus CCR6 (**c**) stainings. FACS contour plots are representative of three or more independent experiments. (**d-h**) Skin (**d-e**), small intestine (**f-g**) and joint (**h**) sections were stained for H&E (**d, f, h**), anti-CD3, anti-CD45 and anti-p-STAT3 (**e, g**). Representatives of six technical replicates from three 26-30 weeks old WT*; Cd4-cre* or *Rc3h1-2$^{fl/fl}$*; *Cd4-cre* mice are shown (20x magnification for **d**, **f**, and 4x magnification for **h**, scale bar represents 100 µm), and CD3$^+$, CD45$^+$ and p-STAT3$^+$ cells are quantified **(e, g)**. Results represent mean ± SEM, with the indicated p-values, * P<0.05 (unpaired, two-tailed t test). (**i**) FACS-analyses of IL-17A versus IFN-γ in PMA and ionomycin-stimulated CD4$^+$ T cells from small and large intestine of 12-18 weeks old WT*; Cd4-cre* and *Rc3h1-2$^{fl/fl}$*; *Cd4-cre* mice. FACS plots are representatives of four independent experiments.

Supplementary Figure S3 Analysis of a Malt1-insensitive roquin mutant.

(**a**) CD4$^+$ T cells from *Rc3h1$^{fl/fl}$; CAG-CAR$^{stop\text{-}fl}$; Cd4-cre* mice were reconstituted with roquin-1^{WT}, roquin-1$^{R510G/R579G}$ or roquin-1$^{1\text{-}510}$ expressed from IRES-GFP co-expressing adenoviruses or infected with empty adenovirus. We analyzed equally infected cells by gating the same expression levels of GFP. The histogram is derived from pregated GFP$^+$ cells. (**b**) Detection of roquin C-terminal and N-terminal cleavage fragments after Malt1 induced cleavage. Immunoblot analysis of roquin expression in CD4$^+$ T cells isolated from wild-type or *Rc3h1$^{fl/fl}$; Cd4-cre* mice. CD4$^+$ T cells were preincubated for 4 h with leupeptin (200 µM), MG132 (25 µM) or with DMSO control. The cells were then stimulated for 60 min (+) with PMA and ionomycin (PMA + iono) or left untreated (-) and cell extracts were analyzed for roquin protein expression in immunoblots by either using the polyclonal roquin antibody (upper panel) or the monoclonal roquin antibody (lower panel). The data is representative of 2 independent experiments.

Supplementary Figure S4 Induced overexpression and deletion of roquin. Stably transduced cells from an *Rc3h1/2$^{-/-}$* MEF cell clone (**a, c**) or from *Zc3h12a$^{-/-}$* bulk MEF cell cultures **(b)** were left untreated or treated with doxycyclin for 16-24 h to induce the expression of roquin-1 and mcherry (**a, c**) or regnase-1 and mcherry (**b**). Cell extracts were analyzed for roquin-1, regnase-1 or tubulin protein expression in immunoblots (**a, b**). Cells were fixed, permeabilized and stained intracellularly with an antibody specific for roquin and analyzed by flow cytometry (**c**). (**d,e**) MEF cells from *Rc3h1-2$^{fl/fl}$; CAG-CAR$^{stop\text{-}fl}$; CreERT2* mice were stably transduced with ICOS expressing retroviruses, that contained the ICOS 3' UTR. The cells were left untreated or were treated with tamoxifen (0.3 µM) for 3 d (**d**) or 4 d (**e**) before roquin protein expression (**d**) or cell surface expression of CAR and ICOS (**e**) were determined by immunoblot (**d**) or FACS analysis (**e**). (**f–h**) Protein expression of

regnase-1 WT and mutant forms in reconstituted regnase-1-deficient MEF cells **(f)**, of roquin-1 WT and mutant forms in reconstituted roquin-deficient MEF cells **(g)** as well as of the ROQ-regnase-1 fusion protein in reconstituted regnase-1-deficient MEF cells **(h)**. Non-transduced WT MEF cells served as control in **(f-g)**. Cell extracts for Western Blots in **(f-g)** were derived from those MEF cell cultures, which were analyzed by FACS in figures 6c, d and f. The data are representative of at least 2 independent experiments.

Supplementary Figure S5 Evaluation of knockdown approaches.

(**a-d**) $CD4^+$ T cells from Tg(DO11.10); Tg(CARΔ-1) mice were transduced with adenoviruses encoding GFP and shRNA against *Zc3h12a, Nfkbiz*, *Nfkbid* or control, as indicated. The $CD4^+$ T cells were cultured under T_H0 conditions for 3d, sorted (**a, d**) or gated on GFP^{high} expressing cells and cell extracts were analyzed for regnase-1 (**a**), IκBζ (**b-c**) or IκBNS (**d**) protein expression by immunoblotting (**a,d**) or by FACS analysis after restimulation by PMA/ionomycin (**b-c**). The data are representative of at least 2 independent experiments.

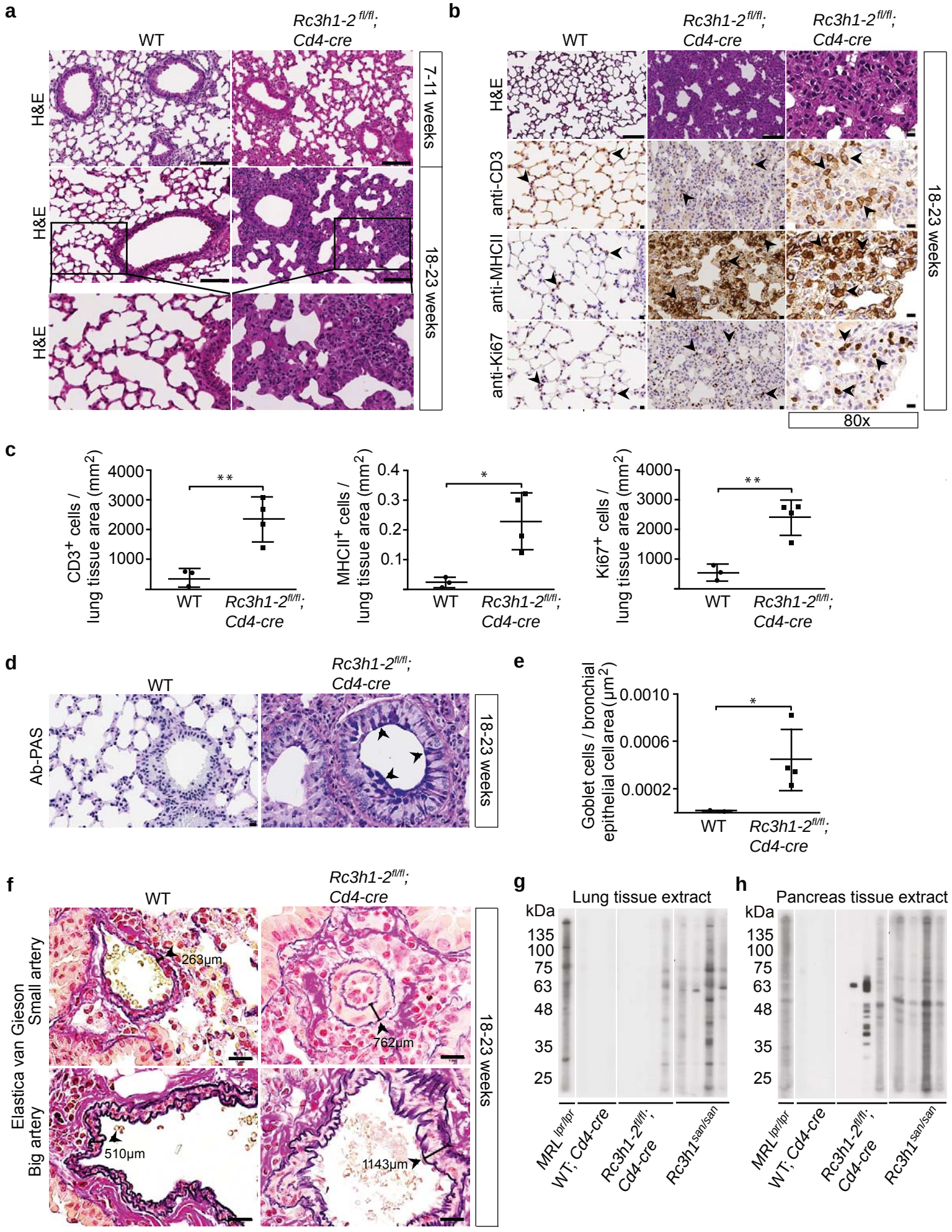

Jeltsch et al., Figure 1

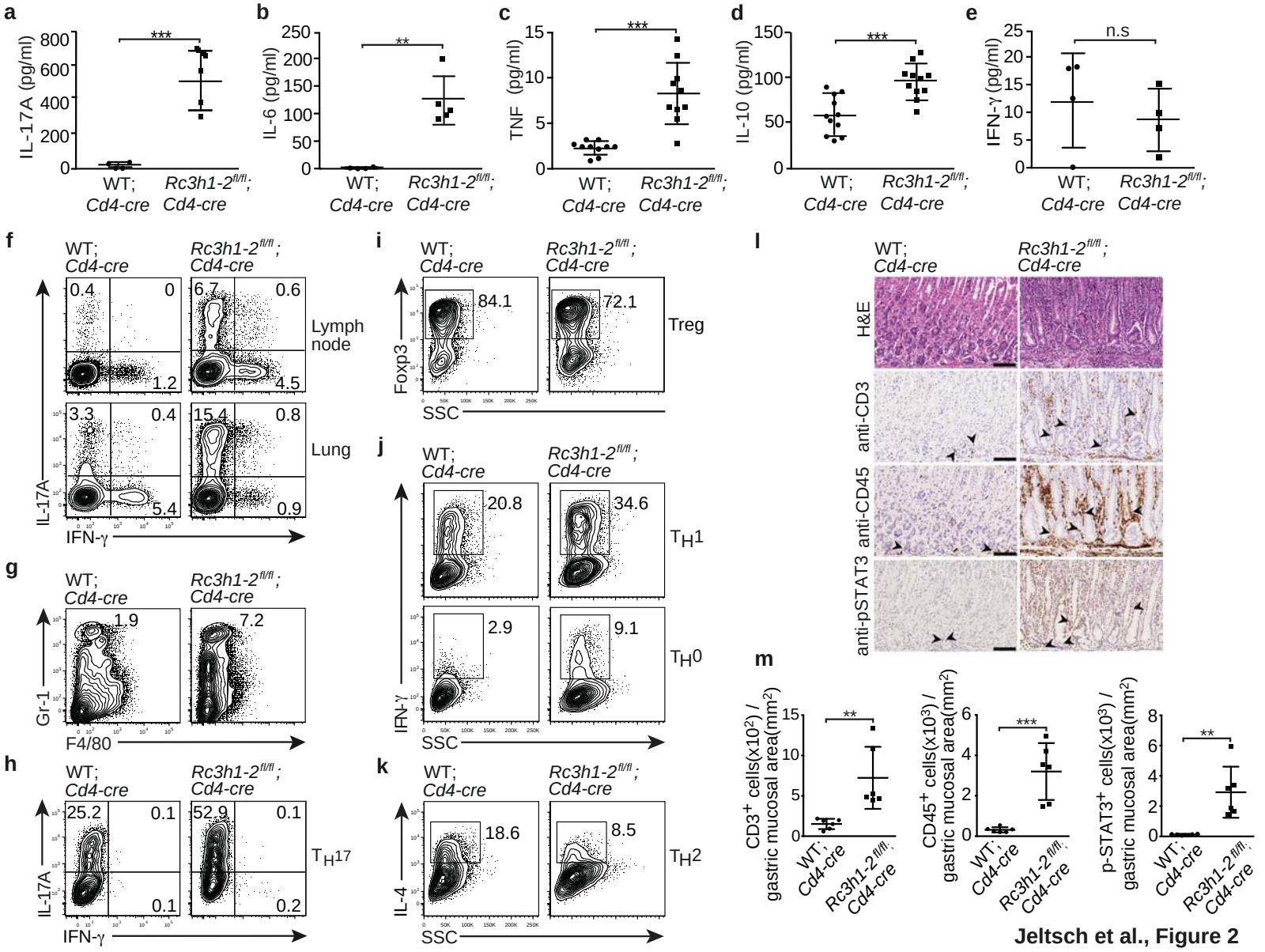

Jeltsch et al., Figure 2

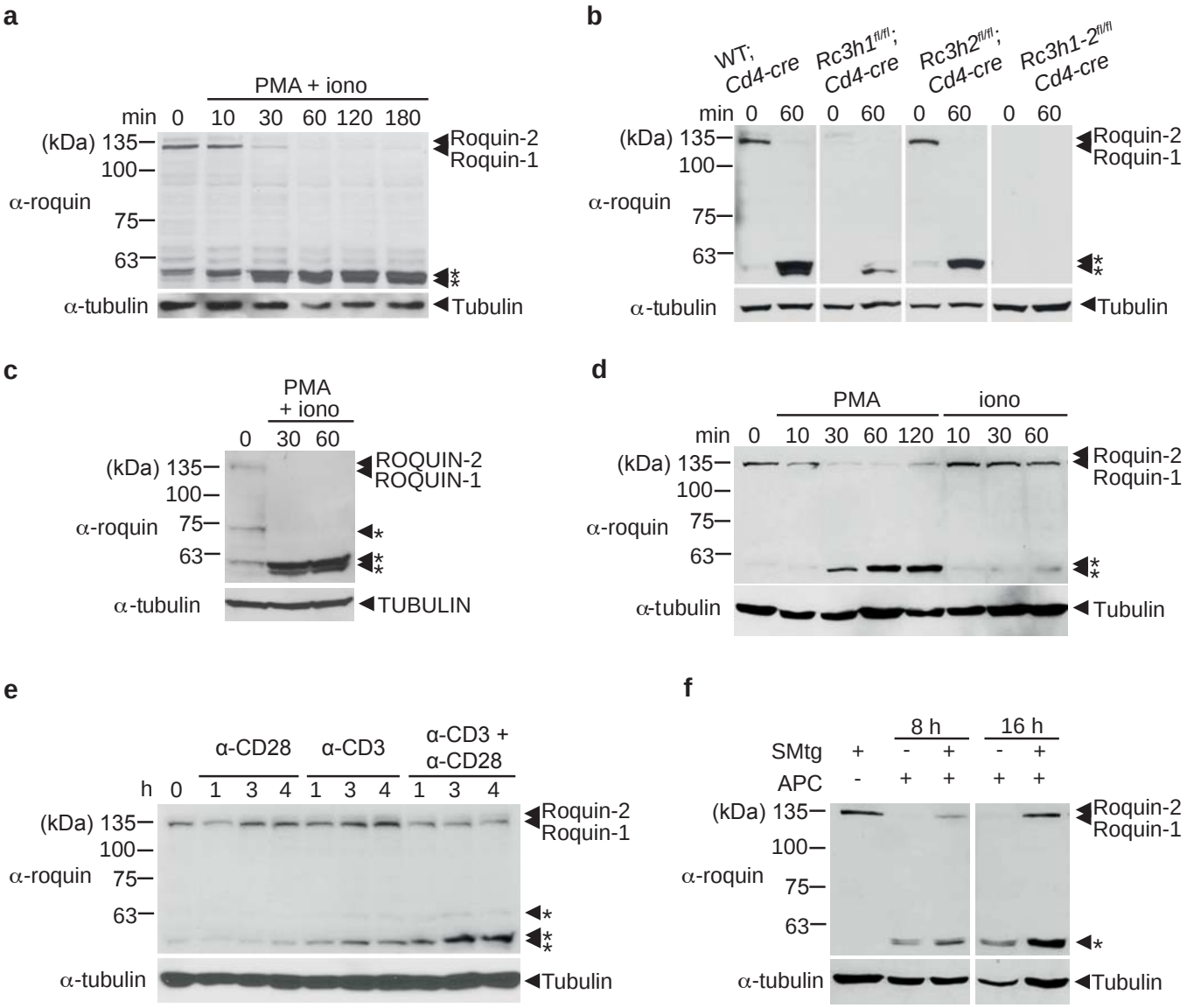

Jeltsch et al., Figure 3

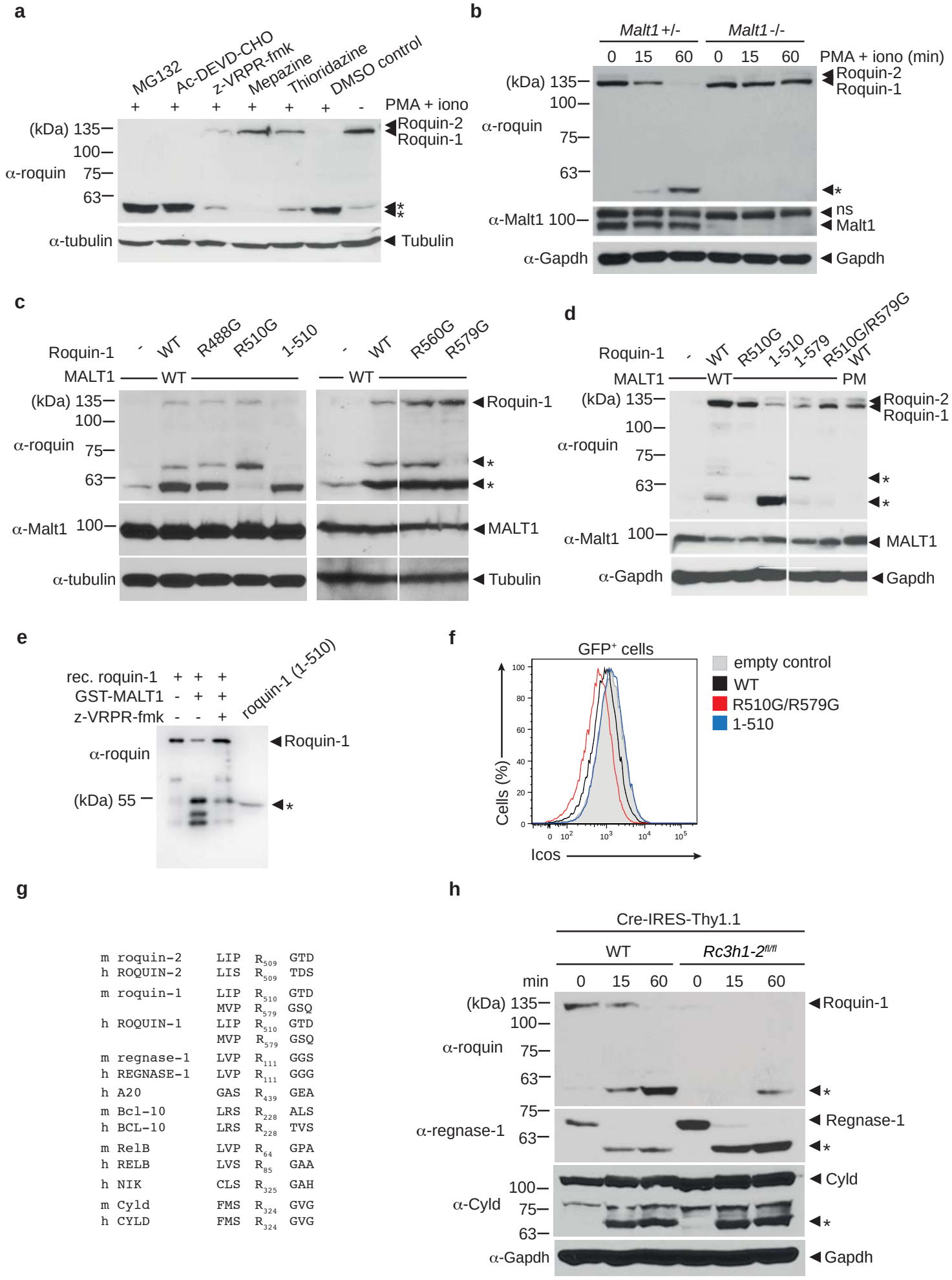

Jeltsch et al., Figure 4

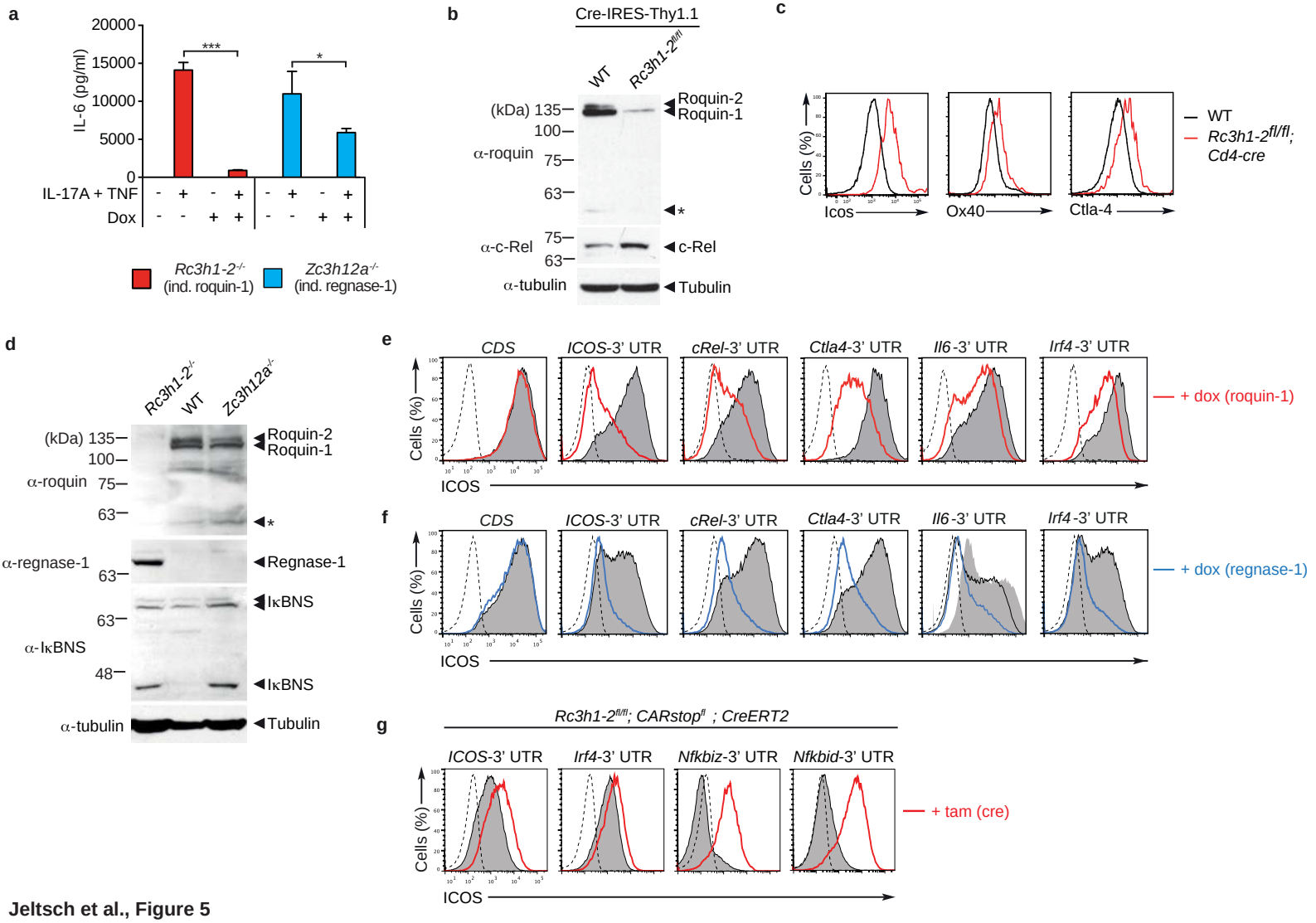

Jeltsch et al., Figure 5

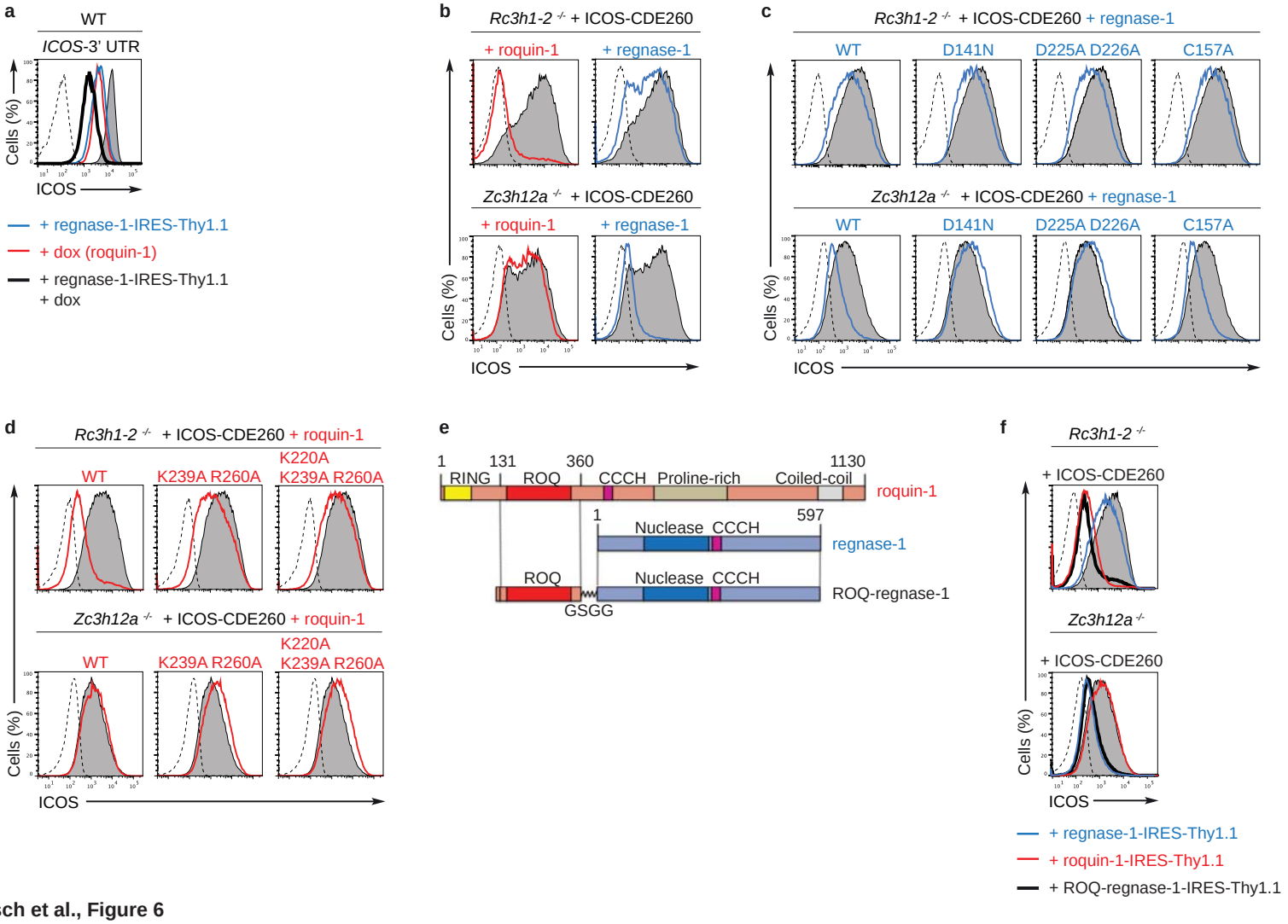

Jeltsch et al., Figure 6

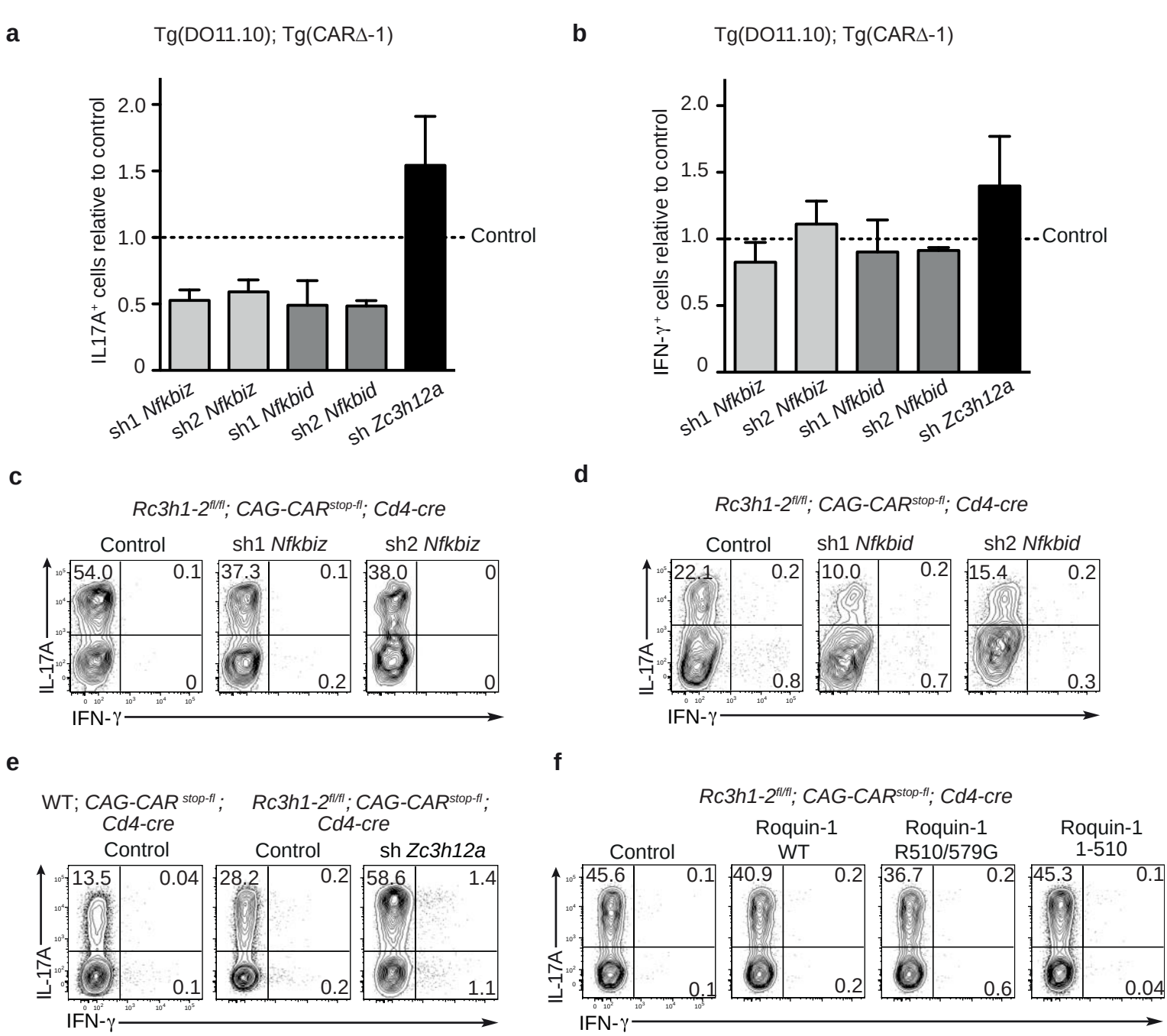

Jeltsch et al., Figure 7

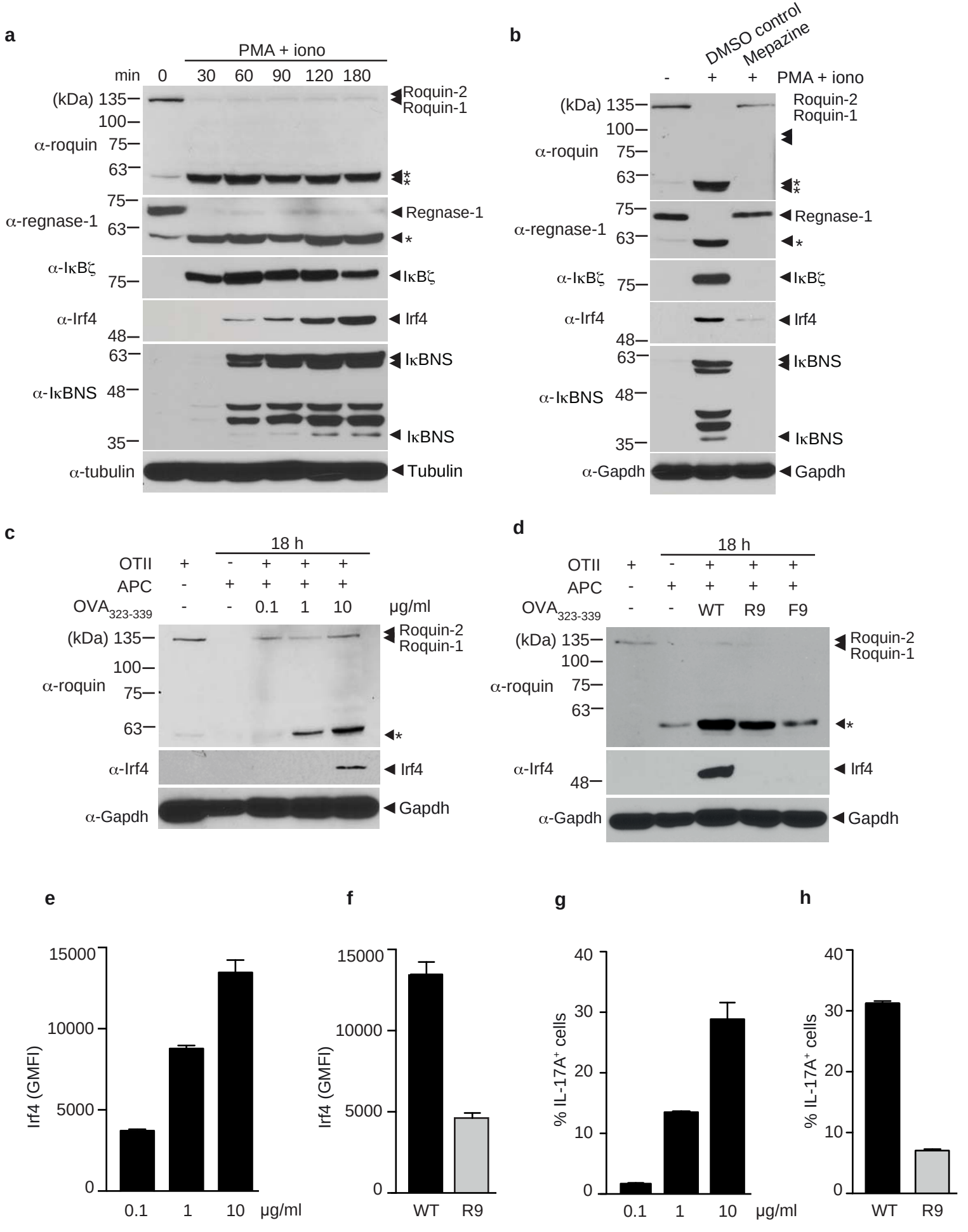

Jeltsch et al., Figure 8